THE ASTROPHYSICAL JOURNAL, 514:148–163, 1999 March 20

A FLUX-LIMITED SAMPLE OF BRIGHT CLUSTERS OF GALAXIES FROM THE SOUTHERN PART OF THE *ROSAT* ALL-SKY SURVEY: THE CATALOG AND log N–log S[1]

S. DE GRANDI,[2,3] H. BÖHRINGER,[2] L. GUZZO,[3] S. MOLENDI,[4] G. CHINCARINI,[3,5] C. COLLINS,[6] R. CRUDDACE,[7] D. NEUMANN,[8] S. SCHINDLER,[2,6] P. SCHUECKER,[2] AND W. VOGES[2]

Received 1998 August 7; accepted 1998 October 29

ABSTRACT

We describe the selection of an X-ray flux-limited sample of bright clusters of galaxies in the southern hemisphere, based on the first analysis of the *ROSAT* All-Sky Survey data (RASS1). The sample is constructed starting from an identification of candidate clusters in RASS1, after which their X-ray fluxes are remeasured using the steepness-ratio technique. This method is better suited than the RASS1 standard algorithm to measuring flux from extended sources. The final sample is count-rate–limited in the *ROSAT* hard band (0.5–2.0 keV), so that as a result of the distribution of N_H, its effective flux limit varies between ~ 3 and 4×10^{-12} ergs cm^{-2} s^{-1} over the selected area. This covers the $\delta < 2.^\circ5$ part of the south Galactic cap region ($b < -20^\circ$), excluding patches of low RASS1 exposure time and of the Magellanic Clouds area, for a total of 8235 deg^2. One hundred and thirty candidate sources fulfill our selection criteria for bona fide clusters of galaxies in this area. Of these, 101 are Abell/ACO clusters, while 29 do not have a counterpart in these catalogs. Of these clusters, 126 (97%) have a redshift, and for these we compute an X-ray luminosity. 20% of the cluster redshifts come from new observations, as part of the ESO Key Program survey of RASS clusters that is currently under completion. Considering the intrinsic biases and incompletenesses introduced by the flux selection and source identification processes, we estimate the overall completeness to be better than 90%. The observed number count distribution, log N–log S, is well fitted by a power law with slope $\alpha = 1.34 \pm 0.15$ and normalization $A = 11.87 \pm 1.04$ sr^{-1} $(10^{-11}$ ergs cm^{-2} s$^{-1})^{\alpha}$, in good agreement with other measurements.

Subject headings: galaxies: clusters: general — surveys — X-rays: galaxies

1. INTRODUCTION

Clusters of galaxies are astrophysical objects that carry fundamental information about the characteristics of the universe. They are the largest gravitationally bound units, and the timescales involved in their dynamical evolution are comparable to the age of the universe. Hence, clusters are cosmologically young structures, in which evidence of initial conditions has not yet been totally removed by dissipative effects. On the other hand, their dynamical state is approaching a characteristic equilibrium configuration that allows coherent modeling (e.g., King 1966). Because of these particular properties, the characteristics of the population of galaxy clusters are strongly related to the cosmological parameters. Both theory and simulations have shown that cluster morphologies, comoving densities, and clustering properties provide information about the density parameter, Ω_0, and the shape and normalization of the primordial power spectrum (e.g., Frenk et al. 1990; Bahcall & Cen 1993; White, Efstathiou, & Frenk 1993; Kitayama & Suto 1997; Evrard 1997).

To be able to measure such ensemble–averaged quantities, one needs to select large, statistically complete samples, which must be representative of clusters of galaxies as a class.

In parallel with deep cluster surveys (e.g., Rosati et al. 1997; Collins et al. 1997; Jones et al. 1998), it is particularly important to accurately define the properties of the cluster population at low redshifts, to provide the reference frame for quantifying cluster evolution. For example, an accurate estimate of the luminosity function, which is an essential part of this statistical analysis, requires the detection of clusters over a fairly large volume of space in order to reach an accurate evaluation of the bright end of the distribution. On the other hand, a sample of clusters of galaxies covering a large volume of the local universe would allow the study of clustering over scales $\gg 100\ h^{-1}$ Mpc, i.e., around the turnover of the power spectrum. On these scales, these measures would overlap the most recent and future microwave background anisotropy experiments (e.g., Gawiser & Silk 1998), thus providing a direct comparison of the clustering in light and mass.

In recent years, it has become ever more evident that the selection of large samples of clusters is best done in the soft X-ray band (i.e., energies in the range of ~ 1 to 10 keV), where clusters are prominent among the various classes of extragalactic objects by virtue of their extremely high X-ray luminosities, $\sim 10^{43}$–6×10^{45} ergs s^{-1} (e.g., Böhringer 1995). The X-ray emission originates in the thin hot gas, contained by the deep cluster potential well, in a state approaching hydrostatic equilibrium (e.g., Sarazin 1988). The predominant emission mechanism at these high energies in clusters is thermal bremsstrahlung, and since the hot gas is distributed throughout the potential well, clusters of galaxies observed in the X-ray band appear, unlike at

[1] Based in part on data collected at the European Southern Observatory, La Silla, Chile.

[2] Max-Planck-Institut für extraterrestrische Physik, Giessenbachstrasse 1, 85740 Garching bei München, Germany.

[3] Osservatorio Astronomico di Brera, via Bianchi 46, 22055 Merate (LC), Italy.

[4] Istituto di Fisica Cosmica, CNR, via Bassini 15, 20133 Milano, Italy.

[5] Università di Milano, via Celoria 16, 20133 Milano, Italy.

[6] Astrophysics Research Institute, Liverpool John Moores University, Byrom Street, Liverpool L3 5AF, UK.

[7] E. O. Hulburt Center for Space Research, Naval Research Laboratory, Code 7620, 4555 Overlook Avenue, Washington, DC 29375.

[8] CEA/Saclay, Service d'Astrophysique, L'Orme des Merisiers Bat. 709, 91191 Gif-sur-Yvette, France.

optical wavelengths, as single diffuse entities. Moreover, since the X-ray intensity scales quadratically with the gas density, whereas the integrated optical luminosity is only linearly correlated with the galaxy density, observations in the X-ray band are less subject to the projection effect problems that affect optically selected catalogs of galaxy clusters.

A unique opportunity to construct large cluster samples selected in the X-ray band has been provided by the *ROSAT* mission (Trümper 1993). In the second half of 1990, this satellite conducted an all-sky survey in soft X-rays (0.1–2.4 keV), with the Position-Sensitive Proportional Counter (PSPC; Briel & Pfeffermann 1986) as the focal-plane detector. Because of their improved spatial resolution, higher sensitivity, and smaller intrinsic background with respect to previous X-ray satellites, *ROSAT* data are especially attractive for the study of clusters of galaxies. Furthermore, the *ROSAT* All-Sky Survey (RASS) is the first to be conducted with an imaging X-ray telescope, and is uniquely suited to obtaining complete X-ray cluster samples over large areas of the sky. Several approaches to the problem of selecting statistical samples of galaxy clusters from the RASS1 database have been described (e.g., Burg et al. 1992; Briel & Henry 1993; Romer et al. 1994; Ebeling et al. 1996, 1997).

In 1992, an ESO Key Program (hereafter ESOKP; Böhringer 1994; Guzzo et al. 1995) was started with the aim of constructing in the southern sky the largest flux-limited sample of clusters of galaxies using the RASS. Because of the huge number of X-ray sources detected (more than 50,000 objects), it was not feasible to start an observing campaign with the aim of optically identifying all the RASS sources in the southern hemisphere. However, it is generally assumed that mass fluctuations on scales of a few to tens of megaparsecs lead to the formation of clusters of galaxies that are visible optically and in the X-ray band. Therefore, the approach followed by the ESOKP collaboration is to search for correlations between X-ray sources and regions of galaxy overdensity. The resulting list is then correlated with catalogs such as the NASA Extragalactic Database (NED) and SIMBAD, in order to remove chance correlations with stars and active galactic nuclei (AGNs). The final step is to observe the refined list spectroscopically, in order to derive the cluster redshift, if not already known, and to remove some remaining sources that are not clusters.

As discussed in De Grandi et al. (1997, hereafter Paper I), however, the standard analysis (see § 2.1) performed on the RASS data is not fully appropriate for characterizing extended sources. In particular, fluxes are systematically underestimated. These limitations have prompted the development of alternative techniques, such as the steepness-ratio technique (SRT), discussed in Paper I, and the Voronoi tessellation and percolation analysis (Ebeling et al. 1996). Here we present an application of the SRT to an initial set of candidate clusters from the ESOKP, which leads to the construction of a complete flux-limited sample of bright clusters of galaxies. The sample is limited to the southern Galactic cap region ($b < -20°$, $\delta < 2.^{\circ}5$), and its X-ray and optical completeness are investigated in detail. In addition, we also compute and discuss the log N–log S distribution.

A preliminary version of the sample presented here was previously used to obtain an estimate of the cluster X-ray luminosity function (XLF; De Grandi 1996b). An updated estimate of the XLF from the present catalog is the subject of a parallel paper (De Grandi et al. 1999). These results will be extended by the future developments of the ongoing ESOKP collaboration (now known as the REFLEX Cluster Survey; see Böhringer et al. 1998).

This paper is organized as follows. In § 2 we briefly describe the RASS1 data used to derive the X-ray source properties and the various algorithms applied to these data. In § 3 we describe the initial procedures used by the ESOKP collaboration to define a sample of clusters in the southern hemisphere using the RASS1 data, which we here call the RASS1 Candidate Sample. The procedure for the selection and definition of the sample of bright clusters, which we call the RASS1 Bright Sample, is presented and discussed in detail in § 4. In § 5 we compute the number counts, or log N–log S distribution, of this sample, and compare it with previous results. In § 6 we investigate the potential biases that could affect the RASS1 Bright Sample. In § 7 we summarize our main results and conclusions.

2. ANALYSIS OF *ROSAT* ALL-SKY SURVEY SOURCES

2.1. *SASS1 Analysis of Strip Data*

The first analysis of the *ROSAT* All-Sky Survey sorted the data into 90 great-circle strips on the sky, each 2° wide and passing through the ecliptic poles. These strips were processed one by one using the Standard Analysis Software System (SASS1; e.g., Voges 1992) developed at MPE (Germany). The detection process used photons in the broad PSPC energy band 0.1–2.4 keV. Each data strip was analyzed using a combination of source-detection algorithms, including two *sliding window* techniques (the first using a local background determination, the latter a global background map) and a maximum-likelihood (ML) method (Cruddace, Hasinger, & Schmitt 1988). SASS1 produced an all-sky source catalog of $\sim$50,000 objects (with existence likelihood larger than 10), containing information about source properties such as detection significance, count rate, position, hardness ratio, and extent. As explained in § 3, the first candidate sample for the ESOKP, on which the present work is based, was selected from this catalog.

2.2. *Analysis of Merged Data*

As mentioned in the Introduction, our first goal was to use the SRT approach to reestimate the X-ray fluxes for all candidate clusters selected from the SASS1 source list. After the end of the survey, it was possible to obtain from the *ROSAT* team 2° × 2° sky fields, centered on the SASS1 ML positions, containing the photons accumulated from all the overlapping strips, known as *merged data*. We collected the merged data fields for all our cluster candidates and first analyzed them using the standard detection procedure, as implemented in the EXSAS package.[9] The first aim of this procedure was to reestimate the source positions with the ML algorithm with improved accuracy. Standard analysis of the merged data was performed in the three *ROSAT* PSPC energy bands: the broad band (0.1–2.4 keV), the soft band (0.1–0.4 keV), and the hard band (0.5–2.0 keV). A detailed description of this analysis can be found in Paper I.

We then proceeded by applying the SRT to the merged data using the new ML position. We recall here that SRT uses the convolution between the real RASS point-spread function (G. Hasinger 1995, private communication) and a

[9] EXSAS User's Guide is available at: http://wave.xray.mpe.mpg.de/users-guide.

β-model of the cluster emission profile (with the parameter β fixed at 2/3), $\tilde{I}(r)$, to derive for each cluster the core radius and the total count rate. We compute for each source the observed steepness ratio, SR_{obs}, which is the ratio between the source counts within an annulus bounded by two radii of 3′ and 5′ and those within a 3′ radius circle. The source core radius is derived by comparing SR_{obs} with the theoretical $SR = \int_{3'}^{5'} 2\pi r\tilde{I}(r)\,dr / \int_{0'}^{3'} 2\pi r\tilde{I}(r)\,dr$ as a function of the core radius (see Fig. 5 in Paper I). The total source counts are computed by correcting the measured counts within a 5′ radius by the fraction falling outside this aperture, by means of an SR_{obs}-dependent correction factor F, shown in Figure 8 of Paper I. The SRT also evaluates the probability that each source will be pointlike, which is computed without using a specific model for the source emission profile. The SRT analysis was performed in all three *ROSAT* PSPC energy bands.

3. THE RASS1 CANDIDATE SAMPLE

As soon as the *ROSAT* All-Sky Survey went through its first processing (SASS1), an automatic identification program for galaxy clusters in the southern sky was set up as a collaboration between MPE and ROE/NRL. The broad aim of this work was to identify all SASS1 X-ray sources that could possibly be associated with a cluster of galaxies, known or unknown, from available optical cluster catalogs. Given the detection limit of the RASS, the redshift distribution of the identified clusters was expected to peak between $z = 0.1$ and 0.2, so that the bulk of the rich cluster population was clearly detectable on the ESO/SRC survey plates.

The main identification method was therefore to look for overdensities of galaxies in the ROE/NRL object catalog, produced by digitizing the IIIa-*J* plates with the COSMOS machine in Edinburgh (Yentis et al. 1992) around each SASS1 source above a given SASS1 count rate (see below). An excess probability could thus be defined by comparison with counts at random positions, and well-characterized thresholds in completeness and contamination could be defined.Relatively low search thresholds in contamination were used to avoid discarding genuine X-ray clusters, leading to the inclusion in the candidate list of some spurious objects that had to be removed in a later step of the work. As a further complement, the SASS1 source list was also correlated with the Abell/ACO catalog of clusters of galaxies (Abell, Corwin, & Olowin 1989) and with a catalog of automatic clusters independently constructed from the COSMOS galaxy database.

The third method was to also include all the sources flagged by SASS1 as having an extent radius $>25''$ and an extent likelihood >7. This is the only method that is based on the X-ray properties alone. Its main drawback is that it is not particularly robust, so some truly extended sources are not recognized as such. In addition, the RASS data are not in general optimal for recognizing extended sources, because of the low photon statistics that couples with the limited resolution of the RASS. Despite its limitations, however, this technique complements the optically based methods, and (see § 6.2) provides a useful way to roughly estimate the completeness of the identification process. Finally, the three cluster candidate lists were merged, and multiple X-ray detections of the same object were removed, for a total of $\sim$1000 objects. In this paper we consider only southern sky candidates at high Galactic latitudes, $\delta < 2.^{\circ}5$ and $b < -20^{\circ}$, leading to a sample of 679. This list will be referred to as the RASS1 Candidate Sample.

As mentioned above, prior to the identification procedure, the initial sample of sources from RASS1 was thresholded to a count-rate limit of 0.055 counts s^{-1}. Because of a problem in the early processing of the data, however, the count rate in a few strips had a systematic shift, so that in the end they were thresholded to a higher limit, 0.08 counts s^{-1}. This problem, discovered later in the course of our analysis, affected 17% of the total sample. We show in the following section how this residual incompleteness has been taken into account.

4. SELECTION OF THE RASS1 BRIGHT SAMPLE

In this section we describe how we proceeded in selecting a flux-limited sample of clusters of galaxies from the RASS1 Candidate Sample. To this end, we must first consider the possible sources of incompleteness that could affect the sample.

4.1. *Exposure Times and Sky Area Selections*

The first source of incompleteness derives from the differences in exposure times over the different strips, which in the southern sky can vary between 0 and $\sim$800 s, with a peak at $\sim$400 s. In Figure 1 we plot the SASS1 broadband count rates versus the SASS1 exposure times for the RASS1 Candidate Sample. We separate the pointlike sources (*asterisks*) from the extended ones (*open circles*) by using the SRT probability of extension: we define as extended any source with a probability $<1\%$ of being pointlike. The solid and dotted lines in Figure 1 correspond to the count-rate limits of 0.055 counts s^{-1} and 0.08 counts s^{-1}, respectively, discussed at the end of § 3. Note that for both count-rate limits, SASS1 starts to fail to detect sources when the exposure time becomes smaller than $\sim$100–120 s. Therefore, we consider only regions with exposures larger than 150 s, in order to avoid regions of the sky where objects could have been missed because of the low sensitivity of the survey.

To avoid incompleteness problems related to the difficulty in identifying clusters inside optically crowded fields,

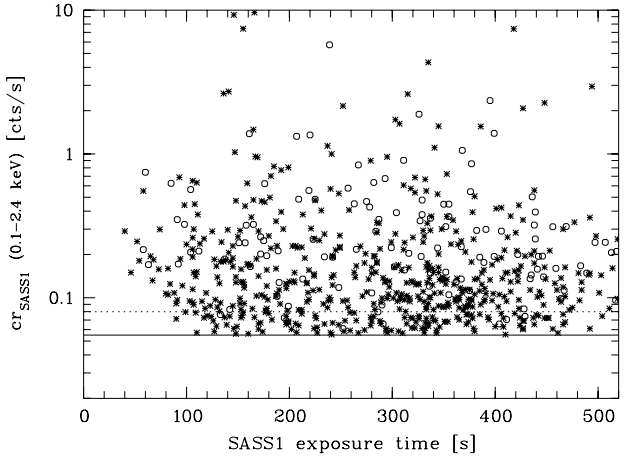

FIG. 1.—SASS1 broadband count rates vs. SASS1 exposure times for the RASS1 Candidate Sample. Sources that were found to be pointlike with the SRT are indicated with asterisks, while sources that were found to be extended are indicated by open circles. The dotted and solid lines represent the limiting SASS1 count rates of 0.08 and 0.055 counts s^{-1}, respectively.

we also excluded the sky areas of the Galactic plane and the Magellanic Clouds. The Galactic plane region had in fact already been excluded in the early selection of the RASS1 Candidate Sample, when configuring to avoid regions of high N_H values by selecting only sources with $b < -20°$. To establish the size of the area to be excluded in the case of the Magellanic Clouds, we considered both the optical and the X-ray cloud emission (e.g., Snowden & Petre 1994). We opted for a conservative choice, rejecting an area slightly larger than that covered by both the emissions.

The lower left and upper right corners of the excluded areas in equatorial coordinates (J2000.0) are $\alpha_{ll} = 93.^{\circ}135$, $\delta_{ll} = -77.^{\circ}5167$ and $\alpha_{ur} = 60.^{\circ}1783$, $\delta_{ur} = -62.^{\circ}3611$ for the LMC, and $\alpha_{ll} = 22.^{\circ}663$, $\delta_{ll} = -77.^{\circ}243$ and $\alpha_{ur} = 353.^{\circ}223$, $\delta_{ur} = -67.^{\circ}224$ for the SMC, respectively.

After excluding these areas and setting a threshold for the exposure time, we are left with the geometric area of 8235 deg^2 (i.e., 2.5 sr), that is shown in Figure 2. This is about one-fifth of the whole sky, or one-third of the sky available at $|b| > 20°$. The number of cluster candidates in this area is 540.

4.2. *Count-Rate Selection*

In § 3 we discussed how the RASS1 Candidate Sample was selected, starting from the list of X-ray sources detected in the survey by SASS1. However, this initial selection procedure was lacking in two respects. First, a flux threshold should be set using count rates in the *ROSAT* hard band (0.5–2.0 keV), which is best suited to the analysis of hard sources such as clusters, whereas initially thresholds were set using SASS1 count rates in the broad band (0.1–2.4 keV). Second, the SASS1 algorithm, designed for speed, was rather imprecise in estimating the flux and angular extent of clusters (Paper I; Ebeling et al. 1996), a problem that the SRT algorithm was designed to correct. In this section, we select bright clusters from the RASS1 Candidates Sample by means of a cut in the SRT count rate computed in the hard band. We show that a limiting SRT count rate of 0.25 counts s^{-1} leads to a sample characterized by a high degree of completeness.

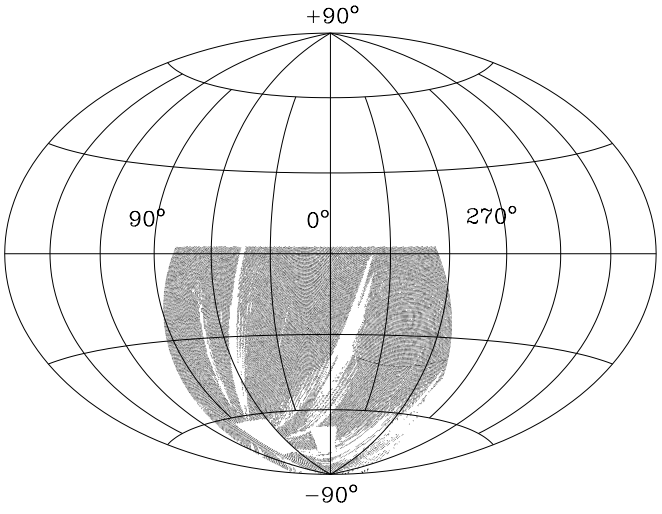

FIG. 2.—Total sky area covered by the RASS1 Bright Sample in equatorial coordinates (J2000.0). Regions with low exposure times (<150 s) and the Magellanic Clouds are shown in white.

4.2.1. *Study of a Control Sample*

In order to understand the effects of changing the energy band and introducing a further count-rate selection using SRT results, we investigate the behavior of a control sample of sources, obtained from the *Einstein* Extended Medium-Sensitivity Survey (EMSS) (Gioia et al. 1990; Maccacaro et al. 1994) and reobserved in the RASS. No cut in SASS1 count rates has been applied to this data set. Out of the 835 EMSS objects, we selected two samples, the first comprising pointlike sources, i.e., objects classified as AGNs, BL Lac objects, and stars (Maccacaro et al. 1994), and the second comprising potentially extended sources, i.e., objects classified as galaxies or clusters of galaxies. For both samples, we include only objects detected in the RASS1 merged data by the ML algorithm (see § 2.2) in the broad band, with an ML existence likelihood larger than 12. These selections lead to well-defined EMSS control samples of 108 pointlike and 50 potentially extended objects.

In Figure 3 we show the comparison between the SRT hard-band count rates and the SASS1 broadband count rates for the EMSS pointlike (*asterisk*) and potentially extended (*open circles*) sources. The observed distribution allows us to estimate how many sources would be lost in passing from one X-ray analysis system to the other. The sources lost as a result of the SASS1 count-rate cut applied prior to the SRT analysis should fall in the top left quadrant delimited by the dotted vertical and horizontal lines representing the cuts of 0.055 counts s^{-1} and 0.25 counts s^{-1}, respectively. Since no pointlike sources are present in the top left quadrant, we deduce that the degree of completeness of a sample of pointlike sources with a threshold in the SRT hard-band count rate of 0.25 counts s^{-1}, previously cut with a SASS1 broadband count rate of 0.055 counts s^{-1}, is extremely high. Two "extended" objects fall in the top left quadrant, indicating that the completeness of the corre-

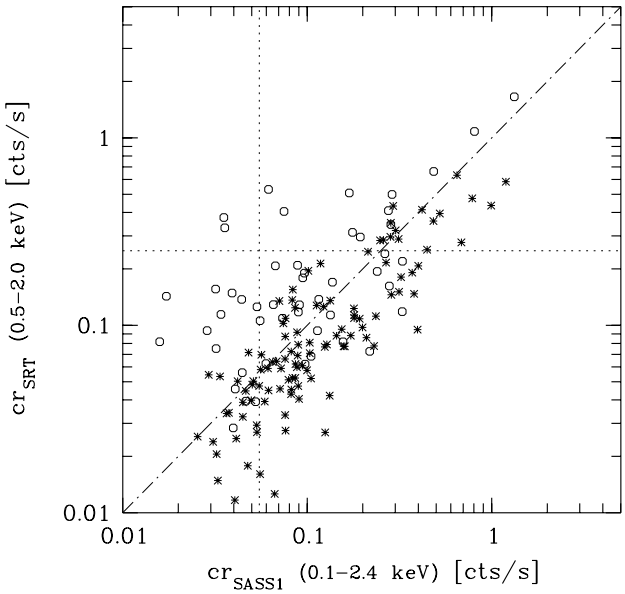

FIG. 3.—SRT hard-band count rates vs. SASS1 broadband count rates for the EMSS control sample. Asterisks indicate pointlike objects (i.e., AGNs and stars), open circles indicate potentially extended sources (i.e., galaxies and galaxy clusters). The vertical and horizontal dotted lines represent the SASS1 count rate limit, 0.055 counts s^{-1}, and the SRT count rate limit, 0.25 counts s^{-1}, respectively. The dot-dashed line shows the bisector of the count-rate plane.

sponding sample of extended sources, although still quite high, is not 100%. The difference between the distributions of pointlike and extended sources in the count-rate plane is produced by the strong underestimation by SASS1 of the count rate for extended sources (see § 4.2).

4.2.2. *Study of the RASS1 Candidate Sample*

In light of the results described above, we now examine our list of cluster candidates. As we mentioned in § 3, this is divided into two distinct subsamples, characterized by two SASS1 broadband count-rate limits (0.055 and 0.08 counts s^{-1}). We call the first sample SUB1 and the second SUB2. SUB1 is not only deeper but also more populated (83% of the total RASS1 Candidate Sample). In Figure 4, we plot for SUB1 the SRT hard band against the SASS1 broadband count rates. The horizontal and vertical dashed lines correspond to count-rate limits of 0.25 and 0.055 counts s^{-1}, respectively. The sources we miss when cutting the SUB1 sample at an SRT hard-band count rate of 0.25 counts s^{-1}, because of the prior SASS1 cut, are those that would populate the top left quadrant. We have used the observed distribution of points in Figure 4 to estimate the number of missed sources. After selecting the SUB1 sources with $cr_{SRT} > 0.25$ counts s^{-1} (133 sources), we have plotted the distribution of their SASS1 count rates. This is shown in logarithmic bins in Figure 5. The histogram has a maximum for $cr_{SASS1} \sim 0.25$ counts s^{-1}, and clearly the decrease below this value is produced by the applied SRT cut. The number of missed sources in the top left quadrant of Figure 4 can then be estimated by extrapolating the distribution below the cr_{SASS1} cutoff. A linear extrapolation, using the four bins nearest to the SASS1 limit, gives the number of missing sources, equal to $\sim 1.5^{+5.4}_{-1.5}$. In order to be conservative, we will take the upper bound of this result, and assume that 6.9 sources are lost.

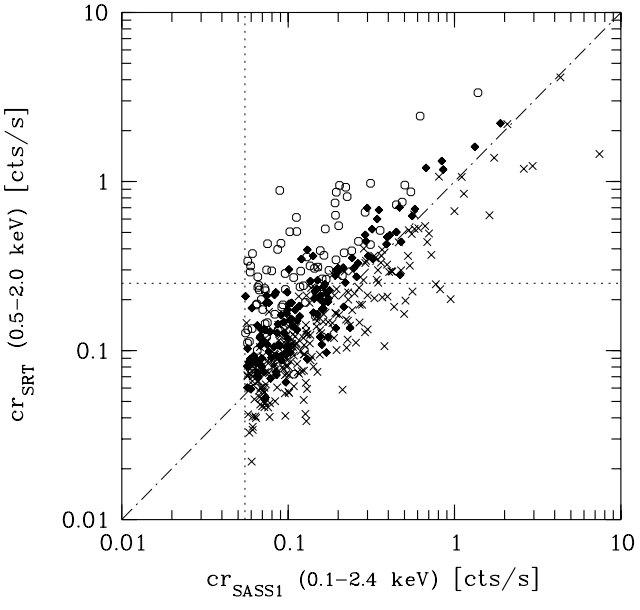

FIG. 4.—SRT hard-band count rates vs. SASS1 broadband count rates for the SUB1 cluster candidate sample (see § 4.2.2 for definition). Crosses show sources with core radii $<1'$, filled squares show sources with core radii from $1'$–$2'$, and open circles show sources with core radii $>2'$. The vertical and horizontal dotted lines represent the SASS1 count-rate limit, 0.055 counts s^{-1}, and the SRT count-rate limit, 0.25 counts s^{-1}, respectively.

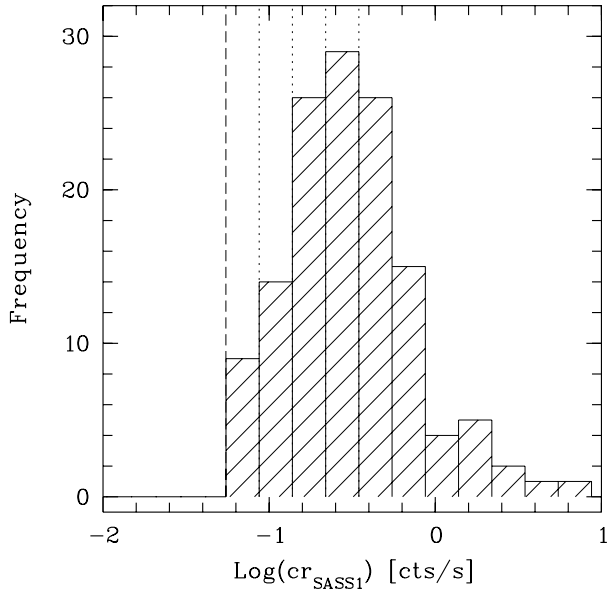

FIG. 5.—SASS1 broadband count rates of SUB1 sources with a SRT hard-band count rate of >0.25 counts s^{-1}. The long-dashed line shows the SASS1 count-rate limit of 0.055 counts s^{-1}; dotted lines show the bins used for the fit (see text for details).

We now wish to estimate the sources we miss when cutting the SUB2 sample at the SRT count rate of 0.25 counts s^{-1}, as a result of the prior SASS1 cut. The number of SUB2 sources above $cr_{SRT} = 0.25$ counts s^{-1} is 31. The number of SUB2 sources that should be falling within the SASS1 count-rate range of 0.055–0.08 counts s^{-1} can be directly estimated from the observed distribution of SUB1 sources: eight objects of SUB1 fall within the SASS1 range 0.055–0.08 counts s^{-1}, corresponding to ~ 1.9 objects in SUB2. The number of SUB2 sources that should be falling below $cr_{SASS1} = 0.055$ counts s^{-1} (i.e., ~ 1.3 objects) can then be derived using the number estimated for SUB1. Adding all these contributions, we estimate that for the whole RASS1 Candidate Sample, the expected missing sources amount to ~ 8.6 (i.e., $\sim 5\%$ of the total sample). We therefore expect the sample to be $\sim 95\%$ complete as far as the X-ray selection is concerned. Such a high degree of completeness has been achieved at the price of drastically reducing the number of sources: the RASS1 Candidate Sample contained 679 objects, while this sample now contains 164 candidates.

4.3. *Definition of the RASS1 Bright Sample*

As a result of the selections described in the previous subsections, we obtain a list of 164 cluster candidates. In order to assign these objects a reliable classification, we have collected the following information: (1) images from the Southern Digitized Sky Survey (SDSS); (2) overlays of X-ray contours on optical object distributions from the COSMOS catalog; (3) information from the NED and SIMBAD databases; (4) X-ray properties, such as source extent, probability of extent, X-ray flux, and luminosity from RASS1 data and *ROSAT* pointed data when available; and (5) optical CCD images and spectra from the ESOKP. Redshifts were obtained from the literature and from our new ESOKP observations.

The analysis of this information allowed us to divide the cluster candidates into four groups:

A. Confirmed clusters of galaxies, i.e., objects for which the inspection of optical images and spectra allow a certain identification of the X-ray source with a cluster.

B. Likely clusters, i.e., objects with X-ray and optical properties consistent with clusters, but lacking firm spectroscopic confirmation.

C. Uncertain identifications, i.e., objects for which we have either insufficient information to discriminate between two possible classifications, or no information at all.

D. Objects that are certainly not galaxy clusters (27 objects).

This classification was done independently three times to reduce subjective definitions, and the agreement was excellent.

The rather high degree of contamination was expected, as a result of the preselection methods we have applied in constructing the RASS1 Candidate Sample.

In Paper I we pointed out that for very extended sources, the source profile appears to be almost flat between 0′ and 5′, and the observed steepness ratio approaches its maximum value (i.e., the ratio between the areas of the annulus bounded by 3′ and 5′ and of the circle of 3′ radius). This large observed steepness ratio leads to diverging values for the core radius, the total source counts, and the associated uncertainties. To overcome this effect, we impose the condition that the physical core radius (in kiloparsecs) of a cluster candidate cannot be larger than a certain upper limit. If the physical core radius found by the SRT is larger than the limit, we compute a new angular core radius from the limiting core radius using the redshift of the source, derive the corresponding steepness ratio (see Fig. 5 in Paper I), and finally, with the new steepness ratio and the curve shown in Figure 7 in Paper I, we compute the revised count rate of the source. The average core radius of rich clusters is about 250 kpc (Bahcall 1975), while Jones & Forman (1984) found that out of 38 clusters, 80% have a core radius smaller than 300 kpc and only 20% have a core radius in the range between 300 and 800 kpc. Various tests with different values of the physical core radius show that the best compromise is achieved with a value of 400 kpc for the upper limit of the core radius. Twenty-one sources belonging to classes A, B, and C have a modified SRT count rate, but for only 14 does the revised count rate differ by more than 10% from its original value. Moreover, seven sources have a revised SRT count rate that falls below our threshold of 0.25 counts s^{-1}, and therefore leave the sample.

We define as the RASS1 Bright Sample the sum of sources belonging to the A (119), B (6), and C (5) groups, using the results of the revised SRT. The final sample contains 130 sources. A schematic representation of the selections leading to the construction of the RASS1 Bright Sample from the RASS1 Candidate Sample is given in Figure 6.

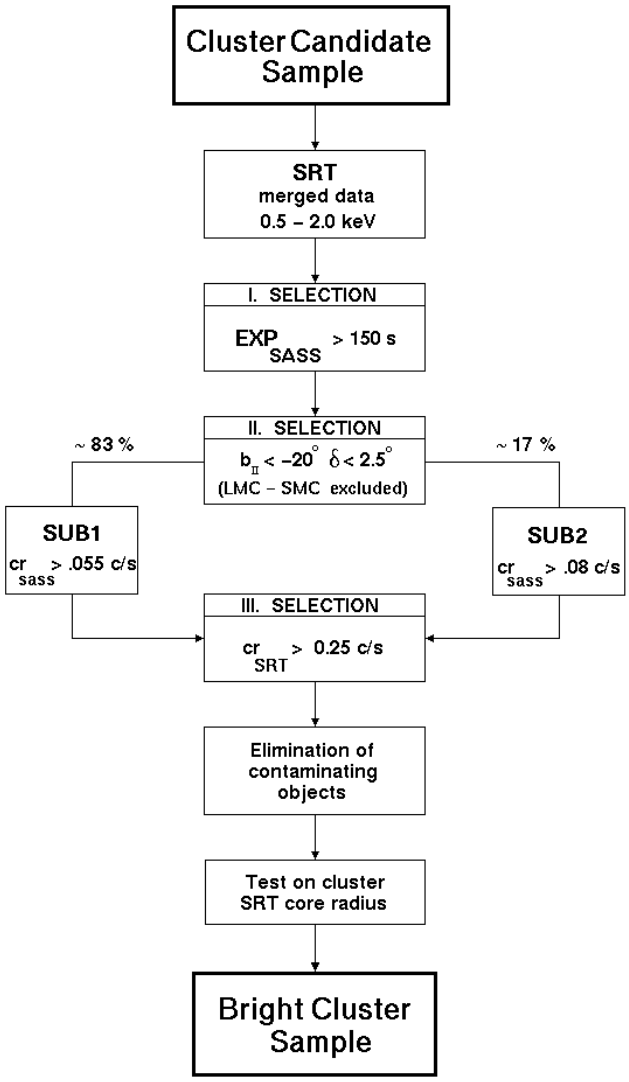

FIG. 6.—Schematic representation of the selections applied to the RASS1 Candidate Sample to obtain the RASS1 Bright Sample.

4.4. *The Catalog of X-Ray Sources*

The sources of the RASS1 Bright Sample are presented in Table 1. Columns list the observed and derived parameters for each source as follows.

Column (*1*).—Sequence number of the source in the catalog.

Columns (*2*) *and* (*3*).—Position; right ascension and declination, as derived by the ML algorithm when analyzing the RASS1 merged data (J2000.0 coordinates).

Column (*4*).—Column density of Galactic hydrogen from Dickey & Lockman (1990), in units of 10^{20} atoms cm^{-2}.

Column (*5*).—Vignetting-corrected RASS1 exposure time, computed from merged data, in seconds.

Column (*6*).—Source count rate, computed in a circle of 5′ radius from the source position in the pulse-height analyzer (PHA) channels from 52 to 201 (corresponding to the 0.5–2.0 keV energy band), with 1 σ errors (in parentheses) from photon-counting statistics.

Column (*7*).—Total SRT source count rate in the 0.5–2.0 keV band, with associated uncertainties.

Column (*8*).—Model-independent probability that the source is pointlike. Sources with probability smaller than 1% are considered extended.

Column (*9*).—Unabsorbed X-ray flux, computed in the 0.5–2.0 keV band in units of 10^{-11} ergs cm^{-2} s^{-1}, with associated symmetrized 1 σ uncertainties (in parentheses).

Column (*10*).—X-ray luminosity, computed in the 0.5–2.0 keV band in units of 10^{44} ergs s^{-1}, with associated 1 σ uncertainties (in parentheses). The luminosity has been computed in the rest frame of the source by assuming a power-law spectrum with energy index 0.4, $H_0 = 50$ km s^{-1} Mpc^{-1}, and $q_0 = 0.5$.

TABLE 1

CLUSTER CATALOG

Sequence (1)	R.A. (J2000) (2)	Decl. (J2000) (3)	N_H (4)	Time (5)	cr, 5′[a] (6)	cr, SRT (7)	P (8)	F_X[a] (9)	L_X[a] (10)	ID (Class) (11)	z (Reference) (12)	Note[b] (13)
001	00 03 09.41	−35 56 22.0	1.09	335.7	0.26 (0.03)	$0.51^{+0.13}_{-0.10}$	9.9E−04	0.62 (0.14)	0.64 (0.15)	A2717 (A)	0.0490 (1)	
002	00 05 59.39	−34 43 05.5	1.16	348.4	0.20 (0.03)	$0.27^{+0.05}_{-0.05}$	4.0E−02	0.34 (0.06)	1.86 (0.33)	A2721 (A)	0.1140 (2)	
003	00 11 20.51	−28 51 05.0	1.84	329.5	0.40 (0.04)	$0.70^{+0.12}_{-0.11}$	3.6E−04	0.88 (0.14)	1.44 (0.23)	A2734 (A)	0.0617 (1)	
004	00 13 37.12	−19 29 54.0	2.00	318.1	0.22 (0.03)	$0.30^{+0.05}_{-0.05}$	4.9E−02	0.37 (0.06)	1.41 (0.24)	A0013 (A)	0.0943 (1)	
005	00 14 20.32	−30 22 58.0	1.65	332.2	0.23 (0.03)	$0.28^{+0.04}_{-0.04}$	1.1E−01	0.35 (0.05)	13.97 (2.16)	A2744 (A)	0.3080 (2)	
006	00 20 44.05	−25 42 21.0	2.26	318.7	0.21 (0.03)	$0.33^{+0.07}_{-0.06}$	1.5E−02	0.42 (0.08)	3.62 (0.72)	A0022 (A)	0.1432 (3)	
007	00 25 34.36	−33 02 43.0	1.69	337.8	0.29 (0.03)	$0.51^{+0.11}_{-0.09}$	1.1E−03	0.64 (0.12)	0.68 (0.13)	S0041 (A)	0.0498 (2)	
008	00 28 35.89	−23 39 07.0	1.82	313.2	0.21 (0.03)	$0.39^{+0.12}_{-0.09}$	4.1E−03	0.49 (0.13)	2.46 (0.65)	A0042 (A)	0.1087 (4)	
009	00 41 50.11	−09 18 17.5	3.58	385.8	1.89 (0.07)	$3.11^{+0.19}_{-0.19}$	3.6E−07	4.09 (0.25)	5.41 (0.33)	A0085 (A)	0.0556 (1)	
010	00 42 08.63	−28 32 09.0	1.49	336.0	0.41 (0.04)	$0.49^{+0.05}_{-0.05}$	1.2E−01	0.61 (0.07)	3.06 (0.33)	A2811 (A)	0.1087 (5)	
011	00 49 24.05	−29 31 21.0	1.80	331.5	0.19 (0.03)	$0.26^{+0.05}_{-0.05}$	5.2E−02	0.32 (0.06)	1.66 (0.32)	S0084 (A)	0.1100 (2)	
012	00 52 34.76	−80 15 21.0	6.64	252.2	0.30 (0.04)	$0.36^{+0.06}_{-0.05}$	1.5E−01	0.52 (0.08)	2.87 (0.43)	A2837 (A)	0.1142 (6)	
013	00 56 11.69	−01 14 52.5	3.10	295.6	0.43 (0.04)	$1.85^{+0.66}_{-0.55}$	1.8E−06	2.41 (5.16)	2.90 (4.32)	A0119 (A)	0.0442 (1)	
014	01 02 42.21	−21 52 43.5	1.60	361.5	0.73 (0.05)	$1.27^{+0.15}_{-0.13}$	1.7E−05	1.58 (0.17)	2.16 (0.24)	A0133 (A)	0.0566 (1)	
015	01 07 49.61	−36 43 43.5	1.86	388.3	0.16 (0.02)	$0.30^{+0.09}_{-0.07}$	6.4E−03	0.37 (0.10)	2.35 (0.64)	A2871 (A)	0.1219 (1)	
016	01 08 13.14	−02 11 33.0	3.01	434.8	0.14 (0.02)	$0.40^{+0.25}_{-0.13}$	1.5E−03	0.52 (0.26)	0.42 (0.21)	A0147 (A)	0.0438 (4)	
017	01 08 52.89	−15 25 45.5	1.69	460.2	0.25 (0.02)	$0.51^{+0.11}_{-0.09}$	1.9E−04	0.63 (0.13)	0.77 (0.16)	A0151 (A)	0.0533 (1)	
018	01 09 52.59	−45 55 42.0	2.10	310.9	0.21 (0.03)	$0.39^{+0.11}_{-0.09}$	4.4E−03	0.49 (0.13)	0.12 (0.03)	A2877 (A)	0.0241 (2)	
019	01 14 59.52	−00 22 13.9	3.32	434.5	0.17 (0.02)	$0.71^{+0.26}_{-0.22}$	2.6E−04	0.93 (2.23)	0.97 (1.92)	A0168 (A)	0.0448 (7)	
020	01 20 58.78	−13 51 07.0	1.85	293.7	0.39 (0.04)	$0.73^{+0.14}_{-0.12}$	3.1E−04	0.92 (0.17)	1.03 (0.19)	0118.5–1408 (A)	0.0511 (8)	1
021	01 25 29.89	−01 45 40.0	3.08	435.1	0.19 (0.02)	$0.30^{+0.06}_{-0.05}$	7.0E−03	0.39 (0.07)	0.05 (0.01)	NGC0533 (A)	0.0171 (6)	2
022	01 31 52.69	−13 36 38.0	1.56	466.4	0.24 (0.02)	$0.33^{+0.05}_{-0.05}$	1.2E−02	0.42 (0.06)	7.43 (1.06)	A0209 (A)	0.2060 (4)	
023	01 37 16.19	−09 11 40.0	2.75	456.7	0.26 (0.03)	$0.51^{+0.11}_{-0.09}$	1.7E−04	0.66 (0.13)	0.44 (0.08)	... (A)	0.0392 (8)	3
024	01 45 07.63	−53 01 58.5	2.35	251.2	0.22 (0.03)	$0.43^{+0.09}_{-0.09}$	5.0E−03	0.55 (0.17)	3.35 (1.03)	A2941 (A)	0.1183 (6)	
025	02 25 52.81	−41 54 46.0	2.14	409.3	0.18 (0.02)	$0.28^{+0.04}_{-0.04}$	7.7E−03	0.35 (0.08)	7.43 (1.53)	A3017 (A)	0.2195 (8)	4
026	02 31 56.22	−01 14 59.5	2.89	256.0	0.08 (0.02)	$0.29^{+2.24}_{-0.17}$	2.3E−02	0.38 (2.05)	0.08 (0.43)	UGC02005 (C)	0.0221 (8)	5
027	02 32 18.69	−44 20 41.5	2.61	388.8	0.22 (0.03)	$0.31^{+0.05}_{-0.05}$	2.0E−02	0.40 (0.07)	13.29 (2.17)	... (A)	0.2836 (8)	6
028	02 49 36.03	−31 11 09.5	1.80	430.7	0.23 (0.02)	$0.37^{+0.06}_{-0.06}$	4.1E−03	0.46 (0.08)	0.10 (0.02)	S0301 (A)	0.0223 (2)	
029	03 03 24.17	−01 56 03.5	7.82	259.7	0.18 (0.03)	$0.26^{+0.06}_{-0.06}$	4.5E−02	0.38 (0.09)	3.79 (0.85)	A0409 (A)	0.1530 (9)	
030	03 07 03.50	−28 40 01.5	1.36	254.3	0.18 (0.03)	$0.26^{+0.05}_{-0.05}$	2.9E−02	0.32 (0.09)	9.15 (2.31)	A3088 (A)	0.2534 (6)	
031	03 14 22.59	−45 25 10.5	3.57	345.7	0.29 (0.03)	$0.46^{+0.08}_{-0.07}$	3.7E−03	0.60 (0.10)	1.32 (0.22)	A3104 (A)	0.0718 (6)	
032	03 17 58.85	−44 14 07.0	2.53	513.0	1.07 (0.05)	$1.38^{+0.08}_{-0.08}$	1.5E−02	1.77 (0.10)	4.24 (0.24)	A3112 (A)	0.0750 (1)	
033	03 28 37.24	−55 42 27.5	3.09	559.7	0.31 (0.02)	$0.44^{+0.05}_{-0.05}$	5.9E−03	0.57 (0.06)	1.79 (0.20)	A3126 (A)	0.0856 (1)	
034	03 30 01.11	−52 35 39.5	1.47	764.1	0.22 (0.02)	$0.44^{+0.08}_{-0.07}$	2.2E−05	0.55 (0.09)	0.72 (0.12)	A3128 (A)	0.0554 (2)	7
035	03 42 53.06	−53 37 43.0	1.06	702.9	0.89 (0.04)	$1.83^{+0.17}_{-0.15}$	1.6E−11	2.25 (0.20)	3.36 (0.29)	A3158 (A)	0.0591 (1)	
036	03 45 58.30	−24 16 45.0	1.58	484.2	0.21 (0.02)	$0.35^{+0.07}_{-0.06}$	2.0E−03	0.44 (0.08)	2.07 (0.36)	A0458 (A)	0.1050 (4)	
037	03 51 25.86	−82 12 44.5	7.65	368.0	0.31 (0.03)	$0.85^{+0.32}_{-0.21}$	3.2E−05	1.25 (0.40)	2.00 (0.64)	S0405 (A)	0.0613 (6)	
038	03 52 25.09	−74 01 02.5	8.02	766.9	0.38 (0.02)	$0.71^{+0.12}_{-0.11}$	4.0E−07	1.04 (0.14)	7.62 (0.96)	A3186 (A)	0.1270 (10)	
039	04 13 59.19	−38 05 50.0	1.41	481.8	0.42 (0.03)	$0.63^{+0.07}_{-0.07}$	1.5E−03	0.78 (0.08)	0.84 (0.09)	1ES 0412-382 (A)	0.0502 (6)	8
040	04 19 39.01	−02 24 24.5	11.5	291.5	0.73 (0.05)	$1.20^{+0.14}_{-0.13}$	1.3E−04	1.93 (0.22)	0.13 (0.01)	NGC1550 (B)	0.0123 (11)	9
041	04 25 51.02	−08 33 38.5	6.40	272.7	0.88 (0.06)	$1.32^{+0.13}_{-0.13}$	7.2E−04	1.87 (0.18)	1.26 (0.12)	EXO 0422-086 (A)	0.0397 (6)	
042	04 30 58.82	−61 27 52.5	1.48	1460.6	0.75 (0.02)	$2.42^{+0.70}_{-0.58}$	1.3E−33	3.00 (1.92)	9.53 (2.85)	A3266 (A)	0.0589 (1)	
043	04 33 37.07	−13 15 20.0	5.68	251.1	1.82 (0.09)	$3.35^{+0.31}_{-0.28}$	6.9E−08	4.65 (0.41)	2.15 (0.19)	A0496 (A)	0.0328 (7)	

TABLE 1—*Continued*

Sequence (1)	R.A. (J2000) (2)	Decl. (J2000) (3)	N_H (4)	Time (5)	cr, 5′[a] (6)	cr, SRT (7)	P (8)	F_X [a] (9)	L_X [a] (10)	ID (Class) (11)	z (Reference) (12)	Note[b] (13)
044	04 45 11.28	−15 51 14.0	4.78	492.3	0.19 (0.02)	$0.65^{+0.42}_{-0.22}$	9.6E−05	0.88 (0.46)	0.50 (0.26)	NGC1650 (B)	0.0363 (12)	10
045	05 00 43.81	−38 40 25.5	3.07	456.0	0.18 (0.02)	$0.50^{+0.25}_{-0.15}$	3.2E−04	0.65 (0.26)	0.80 (0.33)	A3301 (A)	0.0536 (1)	
046	05 10 43.85	−08 01 13.0	8.30	406.3	0.22 (0.03)	$0.31^{+0.05}_{-0.05}$	2.4E−02	0.46 (0.07)	9.30 (1.47)	... (A)	0.2195 (6)	
047	05 25 32.56	−31 36 13.5	1.75	517.0	0.31 (0.03)	$0.54^{+0.08}_{-0.07}$	2.5E−04	0.67 (0.10)	0.41 (0.06)	A3341 (A)	0.0378 (1)	
048	05 28 55.06	−39 27 54.0	2.10	638.2	0.24 (0.02)	$0.30^{+0.03}_{-0.03}$	1.1E−01	0.37 (0.04)	12.54 (1.33)	... (A)	0.2839 (6)	11
049	05 30 35.81	−22 27 56.0	2.57	367.9	0.16 (0.02)	$0.27^{+0.05}_{-0.05}$	3.9E−03	0.34 (0.13)	5.49 (1.65)	A0543 (A)	0.1754 (13)	
050	05 32 23.42	−11 32 03.5	11.1	456.4	0.30 (0.03)	$0.40^{+0.05}_{-0.05}$	3.0E−02	0.63 (0.07)	6.35 (0.73)	A0545 (A)	0.1540 (4)	
051	05 33 14.02	−36 19 10.5	2.93	505.8	0.15 (0.02)	$0.27^{+0.07}_{-0.06}$	3.9E−03	0.35 (0.08)	0.33 (0.08)	S0535 (A)	0.0473 (13)	
052	05 38 15.36	−20 37 34.5	4.00	497.5	0.20 (0.02)	$0.36^{+0.08}_{-0.06}$	1.1E−03	0.47 (0.09)	1.69 (0.33)	A3358 (A)	0.0915 (14)	12
053	05 40 06.82	−40 50 30.5	3.53	601.0	0.43 (0.03)	$0.70^{+0.08}_{-0.07}$	1.0E−04	0.92 (0.10)	0.50 (0.05)	S0540 (A)	0.0358 (2)	
054	05 47 37.44	−31 52 30.0	1.95	579.3	0.31 (0.02)	$0.47^{+0.06}_{-0.05}$	1.2E−03	0.59 (0.07)	5.50 (0.66)	A3364 (A)	0.1483 (6)	
055	05 48 36.70	−25 28 27.0	1.88	553.8	0.26 (0.02)	$0.75^{+0.26}_{-0.18}$	3.9E−06	0.94 (0.28)	0.70 (0.21)	A0548 (A)	0.0416 (1)	
056	05 52 52.08	−21 03 20.5	4.33	529.0	0.33 (0.03)	$0.53^{+0.07}_{-0.06}$	5.3E−04	0.70 (0.09)	2.94 (0.37)	A0550 (A)	0.0990 (6)	
057	05 57 11.89	−37 28 26.0	3.95	705.1	0.21 (0.02)	$0.38^{+0.06}_{-0.05}$	2.3E−04	0.50 (0.08)	0.41 (0.06)	S0555 (A)	0.0440 (6)	
058	06 00 27.27	−48 46 02.0	5.68	993.4	0.27 (0.02)	$0.29^{+0.02}_{-0.02}$	4.1E−01	0.41 (0.03)		... (C)	...	13
059	06 01 37.77	−40 00 31.0	5.01	749.3	0.26 (0.02)	$1.10^{+0.38}_{-0.31}$	1.0E−08	1.50 (2.69)	2.15 (2.38)	A3376 (A)	0.0455 (2)	14
060	06 05 52.68	−35 18 08.0	4.30	714.7	0.38 (0.02)	$0.46^{+0.04}_{-0.04}$	8.7E−02	0.61 (0.05)	5.15 (0.40)	A3378 (A)	0.1410 (15)	15
061	06 21 44.17	−52 42 12.0	5.17	1038.3	0.14 (0.01)	$0.30^{+0.07}_{-0.06}$	5.3E−05	0.41 (0.09)	0.40 (0.09)	MS 0620.6-5239 (A)	0.0480 (10)	
062	06 22 16.78	−64 56 31.5	5.57	3776.8	0.12 (0.01)	$0.32^{+0.05}_{-0.04}$	3.7E−11	0.44 (0.06)	0.11 (0.02)	S0585 (A)	0.0241 (2)	16
063	06 25 42.45	−37 15 02.0	7.08	720.8	0.08 (0.01)	$0.27^{+0.29}_{-0.11}$	2.6E−03	0.39 (0.31)	0.19 (0.15)	A3390 (A)	0.0338 (16)	17
064	06 26 20.10	−53 41 44.5	5.42	1185.9	0.39 (0.02)	$0.95^{+0.13}_{-0.11}$	1.5E−11	1.31 (0.17)	1.58 (0.20)	A3391 (A)	0.0531 (2)	
065	06 27 38.83	−54 26 38.5	5.42	1327.9	0.25 (0.01)	$0.81^{+0.21}_{-0.15}$	8.3E−11	1.12 (0.25)	1.19 (0.27)	A3395 (A)	0.0498 (2)	18
066	06 28 50.19	−41 43 32.5	6.27	633.1	0.23 (0.02)	$0.26^{+0.03}_{-0.03}$	3.2E−01	0.37 (0.04)	4.81 (0.51)	A3396 (A)	0.1759 (6)	
067	06 38 46.66	−53 58 22.0	6.57	861.7	0.28 (0.02)	$0.36^{+0.03}_{-0.03}$	2.7E−02	0.52 (0.05)	10.67 (0.92)	S0592 (A)	0.2216 (6)	
068	06 45 29.21	−54 13 17.5	6.57	723.8	0.24 (0.02)	$0.35^{+0.04}_{-0.04}$	2.8E−03	0.49 (0.06)	5.82 (0.69)	A3404 (A)	0.1670 (6)	
069	06 58 30.41	−55 56 47.0	6.34	507.8	0.35 (0.03)	$0.51^{+0.06}_{-0.06}$	2.2E−03	0.71 (0.09)	27.57 (3.18)	1ES 0657-558 (A)	0.2994 (6)	19
070	19 12 42.19	−75 17 24.0	6.68	218.9	0.26 (0.04)	$0.33^{+0.06}_{-0.06}$	1.2E−01	0.47 (0.09)	1.09 (0.20)	S0810 (A)	0.0736 (6)	
071	19 25 26.27	−42 57 12.5	6.59	301.0	0.25 (0.03)	$0.40^{+0.09}_{-0.08}$	1.0E−02	0.56 (0.12)	1.43 (0.30)	A3638 (A)	0.0774 (6)	
072	19 52 09.89	−55 03 18.5	4.86	191.1	0.20 (0.04)	$0.43^{+0.22}_{-0.14}$	1.3E−02	0.59 (0.25)	0.90 (0.38)	A3651 (A)	0.0599 (1)	
073	20 12 35.08	−56 50 30.5	4.59	174.9	0.91 (0.07)	$2.44^{+0.69}_{-0.50}$	1.6E−06	3.29 (0.81)	4.35 (1.07)	A3667 (A)	0.0556 (1)	
074	20 14 49.98	−24 30 35.0	7.40	367.1	0.20 (0.03)	$0.28^{+0.05}_{-0.05}$	3.1E−02	0.41 (0.07)	4.08 (0.71)	... (B)	0.1538 (6)	20
075	20 18 41.52	−52 42 28.5	4.72	346.3	0.29 (0.03)	$0.55^{+0.12}_{-0.10}$	7.1E−04	0.74 (0.15)	0.80 (0.16)	S0861 (A)	0.0504 (6)	
076	20 22 59.09	−20 57 25.0	5.59	179.6	0.16 (0.04)	$0.25^{+0.10}_{-0.08}$	7.1E−02	0.35 (0.12)	0.48 (0.17)	S0868 (A)	0.0564 (6)	21
077	20 34 19.52	−34 29 12.5	3.90	294.6	0.14 (0.03)	$0.26^{+0.11}_{-0.08}$	2.4E−02	0.35 (0.13)	1.24 (0.45)	A3693 (A)	0.0910 (1)	
078	20 34 41.41	−34 04 16.0	3.90	256.6	0.33 (0.04)	$0.48^{+0.09}_{-0.08}$	1.9E−02	0.64 (0.11)	2.35 (0.41)	A3694 (A)	0.0929 (17)	
079	20 34 46.86	−35 49 07.5	3.56	309.9	0.42 (0.04)	$0.95^{+0.24}_{-0.19}$	4.4E−05	1.25 (0.28)	4.24 (0.96)	A3695 (A)	0.0893 (1)	
080	21 02 10.33	−24 31 59.5	5.33	428.1	0.22 (0.02)	$0.28^{+0.04}_{-0.04}$	7.0E−02	0.38 (0.06)	5.70 (0.81)	EXO2059–247 (A)	0.1880 (18)	
081	21 04 19.81	−41 21 07.0	3.58	354.8	0.21 (0.03)	$0.31^{+0.06}_{-0.06}$	1.7E−02	0.40 (0.08)	4.72 (0.89)	A3739 (A)	0.1661 (6)	
082	21 04 51.57	−51 49 21.0	3.08	278.4	0.37 (0.04)	$0.66^{+0.14}_{-0.12}$	1.1E−03	0.85 (0.16)	0.88 (0.17)	ESO235–G050 (B)	0.0491 (19)	22
083	21 07 07.88	−25 26 40.5	5.52	427.9	0.13 (0.02)	$0.30^{+0.13}_{-0.09}$	3.5E−03	0.41 (0.15)	0.26 (0.10)	A3744 (A)	0.0381 (1)	
084	21 27 05.82	−12 10 12.5	4.78	390.8	0.17 (0.02)	$0.28^{+0.05}_{-0.05}$	2.9E−03	0.38 (0.13)	6.11 (1.71)	A2345 (A)	0.1760 (20)	
085	21 29 40.08	−00 05 49.5	4.22	286.0	0.28 (0.03)	$0.35^{+0.05}_{-0.05}$	8.8E−02	0.47 (0.07)		... (C)	...	23
086	21 36 12.40	−62 22 24.5	3.21	388.4	0.55 (0.04)	$0.67^{+0.06}_{-0.06}$	7.1E−02	0.87 (0.08)		... (C)	...	24
087	21 43 59.42	−56 37 31.0	3.42	353.1	0.35 (0.03)	$0.50^{+0.07}_{-0.07}$	9.3E−03	0.66 (0.09)	1.86 (0.25)	MRC 2140-568 (A)	0.0815 (6)	
088	21 45 54.95	−10 06 24.5	4.03	258.8	0.20 (0.03)	$0.38^{+0.12}_{-0.09}$	8.4E−03	0.50 (0.14)	1.40 (0.40)	A2377 (A)	0.0808 (4)	

TABLE 1—*Continued*

Sequence (1)	R.A. (J2000) (2)	Decl. (J2000) (3)	N_H (4)	Time (5)	cr, 5′[a] (6)	cr, SRT (7)	P (8)	F_X[a] (9)	L_X[a] (10)	ID (Class) (11)	z (Reference) (12)	Note[b] (13)
089	21 46 23.88	−57 17 22.5	2.57	355.8	0.24 (0.03)	$0.42^{+0.10}_{-0.08}$	2.4E−03	0.54 (0.11)	1.35 (0.28)	A3806 (A)	0.0765 (1)	
090	21 46 55.7	−43 53 21	1.77	312.7	0.27 (0.03)	$0.49^{+0.12}_{-0.10}$	1.6E−03	0.62 (0.14)	1.01 (0.22)	A3809 (A)	0.0620 (1)	
091	21 47 49.08	−46 00 02.0	2.72	304.7	0.20 (0.03)	$0.30^{+0.07}_{-0.06}$	2.1E−02	0.39 (0.08)	0.59 (0.12)	S0974 (A)	0.0596 (2)	
092	21 49 07.24	−30 41 52.5	2.31	370.1	0.26 (0.03)	$0.32^{+0.04}_{-0.04}$	9.4E−02	0.41 (0.06)	2.41 (0.33)	A3814 (A)	0.1177 (5)	
093	21 51 55.91	−15 43 19.0	4.27	250.8	0.11 (0.02)	$0.31^{+0.32}_{-0.14}$	1.7E−02	0.41 (0.33)	0.74 (0.60)	A2382 (A)	0.0648 (4)	
094	21 52 20.92	−19 33 54.5	3.05	349.8	0.36 (0.03)	$0.73^{+0.16}_{-0.13}$	1.1E−04	0.94 (0.18)	3.58 (0.70)	A2384 (A)	0.0943 (4)	
095	21 54 10.21	−57 52 05.5	2.12	362.7	0.44 (0.04)	$0.87^{+0.16}_{-0.13}$	3.0E−05	1.10 (0.19)	2.70 (0.46)	A3822 (A)	0.0759 (1)	
096	21 58 23.58	−60 25 40.0	2.77	375.2	0.19 (0.02)	$0.50^{+0.14}_{-0.12}$	5.3E−04	0.65 (0.42)	1.90 (1.02)	A3825 (A)	0.0751 (1)	
097	21 58 30.03	−09 47 54.5	4.00	327.4	0.21 (0.03)	$0.35^{+0.08}_{-0.07}$	7.6E−03	0.46 (0.10)	1.28 (0.28)	A2402 (A)	0.0806 (21)	
098	22 01 50.26	−22 25 53.5	2.61	250.9	0.13 (0.03)	$0.29^{+0.18}_{-0.10}$	1.7E−02	0.37 (0.18)	0.77 (0.38)	S0987 (A)	0.0701 (5)	
099	22 01 58.85	−59 57 37.0	2.84	372.0	0.69 (0.04)	$1.18^{+0.13}_{-0.12}$	2.9E−05	1.52 (0.17)	6.25 (0.69)	A3827 (A)	0.0984 (1)	
100	22 05 39.71	−05 35 00.5	4.68	323.7	0.30 (0.03)	$0.44^{+0.07}_{-0.07}$	1.1E−02	0.60 (0.09)	0.91 (0.14)	A2415 (A)	0.0597 (4)	
101	22 09 25.52	−51 50 37.5	2.06	348.8	0.17 (0.02)	$0.31^{+0.09}_{-0.07}$	6.4E−03	0.39 (0.11)	1.90 (0.51)	A3836 (A)	0.1065 (6)	
102	22 10 20.09	−12 10 49.0	3.87	286.7	0.45 (0.04)	$0.89^{+0.18}_{-0.15}$	1.1E−04	1.17 (0.22)	3.51 (0.66)	A2420 (A)	0.0838 (4)	
103	22 14 32.15	−10 22 23.0	3.86	288.7	0.47 (0.04)	$0.68^{+0.09}_{-0.09}$	5.4E−03	0.90 (0.12)	3.66 (0.47)	A2426 (A)	0.0978 (1)	
104	22 16 16.15	−09 20 11.0	4.50	288.4	0.33 (0.04)	$0.40^{+0.05}_{-0.05}$	1.2E−01	0.54 (0.07)	1.65 (0.22)	A2428 (A)	0.0846 (22)	
105	22 16 56.23	−17 25 25.5	2.28	283.0	0.24 (0.03)	$0.31^{+0.06}_{-0.05}$	6.6E−02	0.40 (0.07)	2.85 (0.49)	... (A)	0.1301 (8)	
106	22 17 45.58	−35 43 21.0	1.10	333.6	0.25 (0.03)	$0.34^{+0.05}_{-0.05}$	3.9E−02	0.42 (0.06)	3.84 (0.59)	A3854 (A)	0.1474 (5)	
107	22 18 07.76	−65 12 00.0	2.83	446.7	0.28 (0.03)	$0.43^{+0.07}_{-0.06}$	3.2E−03	0.55 (0.08)	2.11 (0.31)	... (A)	0.0951 (6)	25
108	22 18 12.49	−03 47 59.0	5.73	253.6	0.18 (0.03)	$0.38^{+0.17}_{-0.11}$	8.2E−03	0.52 (0.20)	1.80 (0.69)	MS 2215.7-0404 (A)	0.0900 (10)	26
109	22 18 40.71	−38 53 46.5	1.33	330.9	0.28 (0.03)	$0.44^{+0.08}_{-0.07}$	4.7E−03	0.54 (0.09)	3.67 (0.63)	A3856 (A)	0.1260 (23)	
110	22 20 33.87	−35 09 52.0	1.09	327.6	0.43 (0.04)	$0.55^{+0.06}_{-0.06}$	4.9E−02	0.67 (0.07)	6.77 (0.75)	A3866 (B)	0.1544 (6)	27
111	22 23 48.91	−01 39 25.0	5.34	237.9	0.29 (0.04)	$0.63^{+0.21}_{-0.15}$	1.4E−03	0.87 (0.25)	3.03 (0.89)	A2440 (A)	0.0904 (4)	
112	22 24 31.31	−55 15 15.0	3.54	362.3	0.15 (0.02)	$0.28^{+0.09}_{-0.07}$	8.8E−03	0.36 (0.10)	0.95 (0.27)	APM 222041.3-552 (A)	0.0780 (24)	
113	22 27 52.46	−30 34 10.5	1.09	312.6	0.42 (0.04)	$0.53^{+0.06}_{-0.06}$	5.7E−02	0.65 (0.08)	0.90 (0.10)	A3880 (A)	0.0570 (23)	
114	22 28 55.32	−60 54 24.5	2.22	458.9	0.13 (0.02)	$0.27^{+0.10}_{-0.07}$	4.6E−03	0.34 (0.11)	0.24 (0.08)	ESO 146-G028 (A)	0.0412 (25)	
115	22 34 28.50	−37 43 53.5	1.20	258.2	0.48 (0.04)	$0.69^{+0.09}_{-0.09}$	8.0E−03	0.85 (0.11)	8.20 (1.08)	A3888 (A)	0.1510 (26)	
116	22 35 39.73	−01 29 02.5	5.81	166.6	0.24 (0.04)	$0.36^{+0.10}_{-0.09}$	4.0E−02	0.51 (0.13)	0.77 (0.20)	A2457 (A)	0.0597 (4)	
117	22 46 17.79	−52 43 48.0	1.52	411.1	0.31 (0.03)	$0.48^{+0.07}_{-0.07}$	2.1E−03	0.60 (0.09)	2.43 (0.35)	A3911 (A)	0.0974 (27)	
118	22 48 44.45	−44 31 50.0	1.79	250.2	0.38 (0.04)	$0.52^{+0.08}_{-0.07}$	2.8E−02	0.65 (0.09)	17.18 (2.49)	S1063 (B)	0.2520[c] (2)	
119	22 50 03.61	−64 26 30.0	2.80	469.6	0.42 (0.03)	$0.93^{+0.20}_{-0.18}$	1.1E−06	1.20 (0.23)	4.69 (0.87)	A3921 (A)	0.0936 (1)	
120	22 54 01.45	−63 15 02.0	2.23	400.2	0.19 (0.02)	$0.28^{+0.06}_{-0.05}$	1.6E−02	0.35 (0.07)	6.62 (1.24)	AM 2250-633 (A)	0.2112 (6)	
121	22 54 27.79	−58 06 41.5	2.12	404.7	0.11 (0.02)	$0.27^{+0.17}_{-0.09}$	7.3E−03	0.35 (0.17)		... (C)	...	28
122	23 13 58.42	−42 43 47.0	1.85	202.4	0.87 (0.07)	$1.07^{+0.10}_{-0.10}$	7.0E−02	1.34 (0.13)	1.93 (0.18)	S1101 (A)	0.0580 (10)	
123	23 15 42.49	−02 22 27.0	4.18	343.1	0.19 (0.03)	$0.30^{+0.07}_{-0.06}$	1.2E−02	0.40 (0.08)	0.12 (0.03)	ZW III 99 (A)	0.0267 (8)	29
124	23 21 36.11	−41 53 37.0	1.96	164.7	0.29 (0.04)	$0.52^{+0.16}_{-0.13}$	1.1E−02	0.66 (0.18)	2.23 (0.62)	A3998 (A)	0.0890 (10)	
125	23 25 18.95	−12 07 32.0	2.50	332.3	0.87 (0.05)	$1.06^{+0.08}_{-0.08}$	5.6E−02	1.36 (0.10)	4.21 (0.31)	A2597 (A)	0.0852 (4)	30
126	23 44 15.98	−04 22 24.5	3.54	339.8	0.40 (0.04)	$0.93^{+0.23}_{-0.18}$	1.8E−05	1.21 (0.27)	3.20 (0.71)	... (A)	0.0786 (8)	
127	23 47 41.78	−28 08 26.5	1.55	334.1	1.30 (0.06)	$2.21^{+0.19}_{-0.18}$	2.0E−06	2.75 (0.23)	1.01 (0.08)	A4038 (A)	0.0292 (1)	
128	23 51 40.36	−26 04 54.0	1.66	329.8	0.43 (0.04)	$0.52^{+0.06}_{-0.06}$	8.8E−02	0.66 (0.07)	14.10 (1.51)	A2667 (A)	0.2264 (8)	31

TABLE 1—*Continued*

Sequence (1)	R.A. (J2000) (2)	Decl. (J2000) (3)	N_H (4)	Time (5)	cr, 5′[a] (6)	cr, SRT (7)	P (8)	F_X[a] (9)	L_X[a] (10)	ID (Class) (11)	z (Reference) (12)	Note[b] (13)
129	23 54 12.70	−10 24 57.0	2.92	317.9	0.34 (0.03)	$0.60^{+0.11}_{-0.10}$	7.8E−04	0.78 (0.14)	1.92 (0.34)	A2670 (A)	0.0762 (1)	
130	23 57 00.02	−34 45 24.5	1.10	350.6	0.96 (0.05)	$1.61^{+0.15}_{-0.15}$	1.3E−05	1.97 (0.18)	1.79 (0.17)	A4059 (A)	0.0460 (10)	

NOTE.—Units of right ascension are hours, minutes, and seconds, and units of declination are degrees, arcminutes, and arcseconds. See text for column descriptions.

[a] Errors are given in parentheses.

[b] Notes on single sources: 1. Cluster in Strubble & Rood 1991. 2. Identified as galaxy MS 0122.9+0129 in Maccacaro et al. 1994, extended from *ROSAT* HRI and PSPC pointed observations; many small galaxies nearby; z measured from three galaxies. 3. Central galaxy is radio source (Brinkman, Siebert, & Boller 1994), z measured from three galaxies. 4. X-ray emission slightly elongated toward cluster A3016. 5. Source at low z (measured on two galaxies), but pointlike; several other objects in the vicinity; could be a group or a single galaxy; uncertain identification. 6. Extended in HRI observation, z measured from two galaxies, RASS data slightly elongated toward a pointlike source at $02^h32^m37^s.5–44^d21^m51^s$ (J2000). 7. Double-peaked X-ray emission; SRT count rate underestimated because the RASS ML position is centered on one peak; 0.61 ± 0.01 counts s^{-1} hard count rate from PSPC pointed observations. 8. Extended in HRI observation; identified as normal galaxy in *Einstein* Catalog IPC Slew Survey, but is a cluster (four galaxies with consistent z). 9. Extended in HRI observation, paired with IC 366 at 3′.2, flagged as a nearby galaxy group in the Lyon-Meudon catalog (Garcia 1993) on the basis of a percolation method; z available only for central galaxy, NGC 1550. 10. Normal galaxy, NGC 1650, in a rich field, likely a galaxy group; only one z available. 11. z measured from four galaxies. 12. Cluster behind star HD 37493 (spectral type K0, $m_V = 8.2$), which could only slightly contribute to the X-ray emission (see Maccacaro et al. 1988); the extended X-ray emission implies that most of the emission comes from the cluster. 13. Unconfirmed cluster with no spectroscopic information available. 14. Elongated X-ray emission between two bright galaxies; SRT count rate in agreement with hard count rate from PSPC pointed observation. 15. Extended in HRI observation. 16. Also A3389 (optical position at 3′.3 from X-ray peak), double-peaked X-ray emission centered on NGC 2235 (at 0′.7). 17. Double-peaked X-ray emission, RASS ML position centered on one peak, 0.27 ± 0.01 counts s^{-1} hard count rate from PSPC pointed observation. 18. Double-peaked X-ray emission, RASS ML position centered on one peak, 1.16 ± 0.03 counts s^{-1} hard count rate from PSPC pointed observation. 19. Extended in HRI observation, classified as a galaxy cluster in Tucker, Tananbaum, & Remillard 1995. 20. Probable cluster, with only one z measured. 21. Central galaxy is a radio source (Brinkman, Siebert, & Boller 1994; Douglas et al. 1996), z measured from two galaxies. 22. Extended in HRI observation, probable group; z only from the brightest galaxy. 23. Extended in HRI observation, no spectroscopic information available. 24. Unidentified candidate, with no spectroscopic information available. 25. z measured from five galaxies. 26. MS 2215.70404 (coincident with RASS ML emission peak) and MS 2216.00401 are two separate sources, probably parts of the extended X-ray emission from a single cluster (Gioia & Luppino 1994). 27. Extended in HRI observation, only one z measured. 28. Probable cluster, no spectroscopic information available. 29. Extended in HRI observation, paired with NGC 7556, z measured from two galaxies. 30. Extended in HRI observation. 31. Extended in HRI observation.

[c] This is an estimated redshift.

REFERENCES.—(1) Mazure et al. 1996; (2) Abell et al. 1989; (3) Dalton et al. 1997; (4) Strubble & Rood 1987; (5) Collins et al. 1995; (6) data from the ESOKP collaboration; (7) Zabludoff et al. 1993; (8) data from the South Galactic Pole survey (see Romer et al. 1994); (9) Crawford et al. 1995; (10) Stocke et al. 1991; (11) de Vaucouleurs et al. 1991; (12) Huchra et al. 1993; (13) Quintana & Ramirez 1995; (14) J. P. Henry & C. R. Mullis 1997, private communication; (15) Ebeling et al. 1996; (16) Galli et al. 1993; (17) Muriel, Nicotra, & Lambas 1990; (18) NED Team 1992; (19) Lauberts & Valentijn 1989; (20) Ledlow & Owen 1995; (21) Postman, Huchra, & Geller 1992; (22) Allen et al. 1992; (23) Ebeling & Maddox 1995; (24) Dalton et al. 1994; (25) Muriel et al. 1995; (26) Teague, Carter, & Gray 1990; (27) Postman & Lauer 1995.

Column (*11*).—Optical identification. Name of the source, if already known, and proposed classification (in parentheses), according to the description given in § 4.3.

Column (*12*).—Source redshift, with associated reference (in parentheses; see table reference note).

Column (*13*).—Comments; contains miscellaneous information on the source.

In Table 2 we list the sources belonging to class D (i.e., noncluster objects discarded from the RASS1 Bright Sample). The contents of Table 2 are:

Column (*1*).—Optical name of the source, if already known.

Columns (*2*) *and* (*3*).—Right ascension and declination (J2000.0) of the X-ray source from RASS1 merged data.

Column (*4*).—Unabsorbed X-ray flux, computed in the 0.5–2.0 keV band with SRT, in units of 10^{-11} ergs cm^{-2} s^{-1}.

Column (*5*).—Uncertainties associated with the X-ray flux, in the same units and energy band as in column (4).

Column (*6*).—Source type: STA = star, GAL = "normal" galaxy, GC = globular cluster, and AGN = active galactic nucleus (quasar, Seyfert galaxy, or BL Lac object).

4.5. *Extent of Clusters in the Catalog*

For each cluster of the RASS1 Bright Sample, we have computed the probability that it will be a pointlike source following the SRT method described in Paper I. We find that about 60% of the clusters belonging to the RASS1 Bright Sample can be confidently defined as extended sources, while the remaining ~40% are consistent with being pointlike. If the RASS1 Candidate Sample had been selected on the basis of source X-ray extent, this would have introduced a severe incompleteness in any flux-limited sample. Indeed, even at a hard-band count-rate limit of 0.25 counts s^{-1} (roughly corresponding to a flux limit of $\sim 3.5 \times 10^{-12}$ ergs cm^{-2} s^{-1}), almost half of the sources would have been lost. This is a consequence of the limited angular resolution of the RASS, in which a significant fraction of the more distant clusters do not appear as extended sources, coupled with the low photon statistics characterizing RASS sources.

5. THE NUMBER COUNTS OF THE RASS1 BRIGHT SAMPLE

5.1. *Converting Count Rate to Flux*

To convert a count rate into an X-ray flux in the 0.5–2.0 keV band, we assume that all clusters have a thermal spectrum (Raymond & Smith model in XSPEC version 9.01), with a temperature of 5 keV, a metal abundance of 0.5 $Z_\odot$, and a redshift of 0.1, which is the median redshift of the RASS1 Bright Sample. The assumption of a spectral model and its associated parameters (T, Z, and z) is not critical, since the flux in the 0.5–2.0 keV band depends only weakly on these parameters. We find that by varying them within a range of values that are typical for clusters of galaxies ($T_{\rm gas} \sim 3$–10 keV, $Z \sim 0.3$–1.0 $Z_\odot$) and for a reasonable redshift range ($z \leq 0.3$), the conversion factor for the *ROSAT* hard band changes by less than 5%.

TABLE 2

REJECTED CLUSTER CANDIDATES

Source ID (1)	R.A. (J2000) (2)	Decl. (J2000) (3)	F_X (10^{-11} cgs) (4)	F_X Error (10^{-11} cgs) (5)	Type (6)
HD 3237	00 35 08.17	−50 20 05.5	0.61	0.08	STA
NGC 0253	00 47 32.70	−25 17 21.0	0.45	0.07	GAL
G60	01 35 00.88	−29 54 40.0	1.54	0.06	STA
	02 27 16.47	+02 01 55.5	1.10	0.08	AGN
2A 0311−227	03 14 12.88	−22 35 41.5	1.81	0.11	STA
MRK 0609	03 25 26.58	−06 08 20.5	0.45	0.04	AGN
HR 1325	04 15 22.25	−07 38 56.5	0.51	0.07	STA
H0449−55	04 53 31.51	−55 52 01.0	0.79	0.05	STA
HR 702	05 12 55.25	−16 12 19.5	0.35	0.06	STA
NGC 1851	05 14 06.18	−40 02 31.0	2.87	0.10	GC
0548−322	05 50 40.53	−32 16 17.5	2.04	0.08	AGN
HD 45081	06 18 27.59	−72 02 40.5	0.74	0.04	STA
HR 2326	06 23 57.31	−52 41 43.0	0.50	0.04	STA
PMN J1931−2635	19 31 50.01	−26 34 31.5	0.45	0.09	AGN
PKS 1930−510	19 34 51.95	−50 52 54.0	0.50	0.54	GAL
HR 7571	19 53 06.63	−14 36 08.0	0.44	0.06	STA
PKS 2005−489	20 09 25.07	−48 49 48.0	1.62	0.09	AGN
PKS 2035−714	20 40 06.08	−71 14 53.0	0.35	0.06	AGN
	20 41 49.71	−37 33 45.0	0.57	0.10	GAL[a]
HD 205249	21 34 16.18	−13 29 07.5	0.54	0.07	STA
PMN J2150−1411	21 50 15.62	−14 10 45.0	0.85	0.10	AGN
ESO 075−G041	21 56 54.04	−69 40 34.5	0.38	0.06	AGN
SAO 145804	22 00 36.51	−02 44 27.0	5.86	0.22	STA
[HB 89] 2227−399	22 30 39.28	−39 42 54.0	0.39	0.05	AGN
NGC 7603	23 18 56.18	+00 14 38.5	0.40	0.04	AGN
HD 220054	23 21 52.89	−69 42 18.0	0.40	0.07	STA
HD 220186	23 21 55.46	−10 50 03.0	0.56	0.06	STA

NOTE.—Units of right ascension are hours, minutes, and seconds, and units of declination are degrees, arcminutes, and arcseconds. See text for explanation of types.

[a] Identification based on *ROSAT* HRI and COSMOS data.

With these assumptions, we find that the relation between count rate and flux as a function of N_H is well fitted, for N_H in the range 7×10^{19}–4×10^{21} cm^{-2}, by a quadratic relation (see also De Grandi 1996a):

$$S = (1.193 + 3.315N_H + 2.152N_H^2)\,\mathrm{cr}\,, \quad (1)$$

where S is the 0.5–2.0 keV flux in units of 10^{-11} ergs cm^{-2} s^{-1}, N_H is the Galactic absorption for the individual cluster as given in Dickey & Lockman (1990) in units of 10^{22} cm^{-2}, and cr is the SRT hard-band count rate.

5.2. *Sky Coverage and* log N–log S *Distribution*

Our sample has been obtained by performing a cut in the count rate. Since different regions of the sky show different amounts of Galactic absorption, the cut in the count rate translates into a range of flux limits. We have computed the flux limit as a function of N_H, and from that we have derived the sky coverage as a function of the flux limit (see Fig. 7). Since regions of high Galactic absorption have been excluded from the RASS1 Bright Sample (§ 4.1), N_H varies within a limited range, $10^{20} < N_H < 10^{21}$ cm^{-2}. Consequently, the flux limit does not vary much over the available sky area, so that the sky coverage (see Fig. 7) is almost constant for flux limits larger than $\sim 4 \times 10^{-12}$ ergs cm^{-2} s^{-1} and decreases rapidly to zero at the flux limit of 3.05×10^{-12} ergs cm^{-2} s^{-1}.

The flux limit should take into account exposure time, and in the case of clusters the angular extent (e.g., Rosati et al. 1995). However, in our case both of these dependencies may be neglected. As long as the exposure time is larger than 150 s (§ 4.1) and the extension is less than $\sim 4'$ (§ 6.1), a source with an SRT hard-band count rate of >0.25 counts s^{-1} will be detected.

The cumulative log N–log S distribution for the 130 objects of the RASS1 Bright Sample has been computed by summing up the contribution of each cluster, weighted by the area in which the cluster could have been detected:

$$N(>S) = \sum_{S_i > S} \frac{1}{\Omega_i}\,, \quad (2)$$

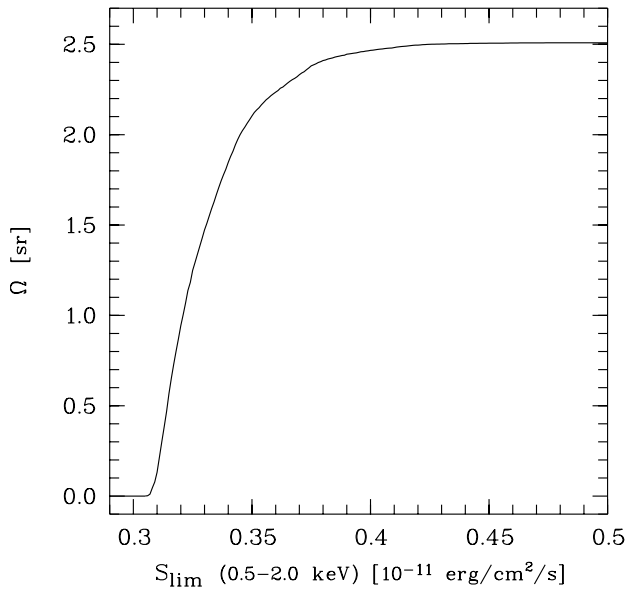

FIG. 7.—Sky coverage as a function of the flux limit for the RASS1 Bright Sample.

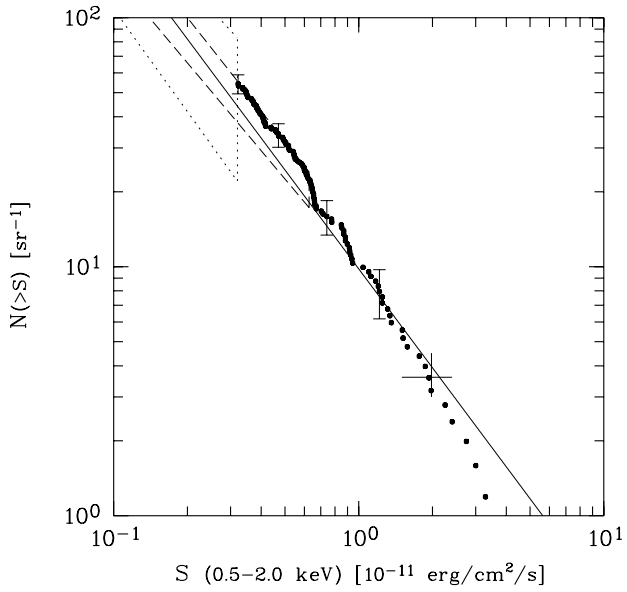

FIG. 8.—Cumulative cluster number counts distribution, log N–log S, of the RASS1 Bright Sample (*filled circles*). Vertical error bars on a few individual points represent the uncertainty in the number of clusters. Also shown, for comparison, are the log N–log S relations of other cluster samples: the long-dashed box represents the EMSS log N–log S (Henry et al. 1992), as recalculated in Rosati et al. 1995; the cross represents the Piccinotti et al. 1982 point; the dotted box shows the extrapolation of the bright end of the RDCS sample by Rosati et al. 1997; and the solid line represents the best-fit of the BCS sample (Ebeling et al. 1998).

where $N(>S)$ is the surface number density of sources with flux larger than S, S_i is the flux of the ith source, and Ω_i is the associated solid angle. The log N–log S distribution is plotted in Figure 8.

We have modeled the log N–log S distribution with a power law of the form

$$N(>S) = AS^{-\alpha}\,, \quad (3)$$

and computed the power law slope, α, using the ML method described in Crawford, Jauncey, & Murdoch (1970) and Murdoch, Crawford, & Jauncey (1973), which uses the unbinned data. The likelihood function, $\mathscr{L}$, is given in the Appendix of Murdoch et al. (1973). The derived value for α (1.37 ± 0.15) has been corrected by the factor $(M-1)/M$ (Crawford et al. 1970), where M is the number of objects in the sample, and for the bias in the derived slope induced by the presence of measurement errors in the fluxes (Murdoch et al. 1973, Table 5). This last correction is computed by Murdoch et al. (1973) for the case of noise-limited flux measurements; however, because of the way our sample has been selected, the minimum S/N ratio is not well defined. On the basis of an analysis of the overall S/N distribution, we have defined an effective limiting S/N (~ 8) corresponding to the peak of the distribution, and we have applied the correction appropriate for this value. The corrected value of the slope is $\alpha = 1.34 \pm 0.15$, where the quoted errors are 1 σ. The cumulative effect of the two corrections shifts the value of the slope by an amount that is much smaller than the errors. We note that the observed slope is consistent within 1 σ with the Euclidean slope. The normalization, A, has been computed by imposing the condition that the integral distribution, $N(>S)$, described by the power law be equal to the observed one at the flux of the weakest cluster in the sample. The derived value is $A = 11.87 \pm 1.04$ sr^{-1} (10^{-11}

ergs cm^{-2} $s^{-1})^{\alpha}$. Since the ML method does not establish whether a model is acceptable, we have applied a Kolmogorov-Smirnov (KS) test to our data. In the case of a power law with slope α equal to that derived above, the KS test yields a probability of 0.77 for the observed distribution to be extracted from the parent population, indicating that a power law adequately describes our data.

If the best-fit power law is drawn over Figure 8, it appears to be above the data for all the fluxes higher than about $0.6–0.7 \times 10^{-11}$ ergs cm^{-2} s^{-1}. This effect is due to the different statistical weight given to the data points by the ML algorithm used for the fitting procedure and to the fact that the distribution reported in Figure 8 is cumulative. Indeed, by plotting the differential log N–log S, this effect disappears, indicating its purely statistical nature.

We have performed an internal consistency test by computing the log N–log S distribution and the best-fit power law for the 119 sources classified as certain clusters (A) only. The best-fit parameters, $\alpha = 1.32 \pm 0.15$ and $A = 11.14 \pm 1.01$, are in agreement with those found by considering the whole sample. Moreover, a KS test between the flux distribution of the sources classified as A and the sources in the B and C groups did not show any evidence of a statistically significant difference between the two subsamples.

Figure 8 also shows a comparison of our log N–log S distribution with other works. The filled circles in Figure 8 show our data, while the long-dashed box and the cross represent the EMSS log N–log S distribution (Henry et al. 1992), as recalculated by Rosati et al. (1995), and the Piccinotti et al. (1982) point, respectively. The solid line corresponds to the number counts of the brightest cluster sample (BCS) (Ebeling et al. 1998, Table 2), and the dotted box corresponds to the extrapolation of the bright end of the ROSAT Deep Cluster Survey (RDCS) sample, as given by Rosati et al. (1997).

Our best fit to the log N–log S distribution is systematically above that found for the BCS sample. The difference at a flux of 3.05×10^{-12} ergs cm^2 s^{-1} is 19% and is significant at about the 2 σ confidence level. Possible explanations for this difference could be the different efficiencies of the preselection methods used in compiling the two cluster samples or the different techniques used to estimate the X-ray fluxes.

Another sample of RASS1 clusters already available in the literature and covering the sky at $|b| > 20°$ is the X-Ray Brightest Abell Clusters (XBACs) sample (Ebeling et al. 1996). This sample, however, is optically selected, since it was compiled by looking for cluster soft X-ray emission over the objects in the Abell and ACO catalogs. Moreover, the *ROSAT* energy band used to derive the X-ray fluxes was the broad band (0.1–2.4 keV).

In general, our data are in good agreement with previous estimates of the log N–log S distribution, and moreover, since both the EMSS and RDCS cluster samples are purely X-ray selected, the good agreement in the number counts suggests that our selection function, which is partially driven by the optical properties of clusters (see § 3), does not lead to a significant incompleteness.

6. COMPLETENESS OF THE RASS1 BRIGHT SAMPLE

In this section we discuss possible sources of incompleteness in the RASS1 Bright Sample, which requires a review of the initial selection process of the RASS1 Candidate Sample.

6.1. *Biases Introduced by the SASS1 Detection Algorithm and the SASS1 Count-Rate Cut*

As stated in § 3, the RASS1 Candidate Sample was selected from the SASS1 source list, and therefore one possible origin of incompleteness is related to the limitations of SASS1 in detecting and characterizing sources. The detection algorithm implemented within SASS1 was optimized to detect pointlike sources. Both the two sliding window and the ML techniques (see § 2.1) use fixed apertures to detect sources, so extended sources with low surface brightness may either not be detected or have their count rates significantly underestimated. Another cause of underestimated source count rates comes from the assumption made within the ML technique that the source brightness profile is a sum of Gaussians, which is not a good description of the profile of most galaxy clusters.

The conservative solution we adopted to effectively limit the incompleteness of the RASS1 Bright Sample with respect to extended sources was to choose a very high limiting count rate. In the following sections, using the distribution of sources in Figure 4, we try to estimate the typical angular dimensions of the objects that may have been lost as a result of the effects described above. From Figure 4 we note that the more extended the source, the farther away it is from the bisector of the count-rate plane (*dot-dashed line*); this is because SASS1 severely underestimates the count rates of the more extended sources. Therefore, the sources that were missed in the RASS1 Bright Sample because they were not detected by SASS1, i.e., those that should fall in the top left quadrant in Figure 4, must be highly extended sources. We have seen that this incompleteness should be limited to $\lesssim 5\%$ (§ 4.2.2). In order to estimate the typical extent of these clusters, we have performed the following quantitative analysis on the data distribution reported in Figure 4. To first approximation, we can relate the distance of any straight line parallel to the one-to-one line with a value of the extension, i.e., the core radius. The sources that should fall in the top left quadrant in Figure 4 must have an extent larger than that corresponding to the straight line parallel to the bisector of the count-rate plane crossing the point $(cr_{SASS1}, cr_{SRT}) = (0.055, 0.25)$. Drawing this line in Figure 4, we see that 11 sources fall above the line, and that all these sources have a core radius larger than about 4′.

Therefore, the ~ 8.6 sources that we estimated in § 4.2.2 as probably missing from the sample because of the flux cuts very probably have core radii of 4′ or larger. Taking a value for the physical core radius of 250 kpc and a Hubble constant of 50 km s^{-1} Mpc^{-1}, we calculate that a cluster with an angular core radius of 4′ would have a redshift of 0.08. Thus, the $\sim 5\%$ incompleteness discussed in § 4.2.2 is most likely due to sources with redshifts smaller than ~ 0.08. This should be treated as a first-order estimate, first because we have used an approximate analysis, and second because clusters show a scatter in their physical core radii.

From a preliminary analysis of the ACO clusters within the area of the RASS1 Bright Sample (Böhringer et al., in preparation), we find that six ACO clusters with hard-band count rates larger than 0.25 counts s^{-1} are missing from our sample. All but one of these clusters were detected from SASS1, but their SASS1 broadband count rates were < 0.055 counts s^{-1}, i.e., below the initial SASS1 count-rate limit of the RASS1 Candidate Sample. All these clusters have a measured redshift $\lesssim 0.06$, in agreement with our

expectations about the bias against the more extended and nearby clusters and our completeness estimate of § 4.2.2. The properties of these six ACO clusters are reported in Table 3:

Column (*1*).—Name of the ACO cluster.

Column (*2*).—Right ascension (J2000), in degrees.

Column (*3*).—Declination (J2000), in degrees.

Column (*4*).—SASS1 count rate, measured in the (0.1–2.4 keV) band.

Column (*5*).—Measured redshift.

Column (*6*).—Redshift reference.

6.2. *Biases Introduced by the Identification Process*

As described in § 3, the RASS1 Candidate Sample was selected using basically two means of identification: the clusters were found either directly by their optical counterparts (overdensities in the COSMOS galaxy catalog, direct or preprocessed; or optical clusters in the Abell and ACO catalogs), or by having been flagged as extended sources during the SASS1 source analysis.

Clearly, this procedure is potentially prone to a number of selection effects, which can be summarized as follows.

1. *Optical counterparts.*—The COSMOS galaxy catalog was produced through the analysis of digitized ESO/SRC *J* survey optical plates (Yentis et al. 1992), using automatic algorithms. One recognized problem of the digitization and star-galaxy separation processes is in the correct treatment of diffraction spikes and halos around bright stars and of the extended envelopes of cD galaxies (Heydon-Dumbleton et al. 1989). For our purposes, it is reasonable to think that this effect will in general increase the contamination of the RASS1 Candidate Sample by including spurious "clusters", but should not reduce its completeness. A more serious concern is the misclassification of galaxies as stars, estimated to be around 5% in the COSMOS data. This could potentially reduce the contrast of a poor cluster and thus exclude it from the sample.

Concerning the use of the Abell and ACO catalogs, one might worry that they are biased against poor systems (expected to be in any case rare in our sample at z larger than ~ 0.04), and affected by subjective biases that are difficult to quantify a priori.

2. *X-ray extension.*—Sources were classified as extended using the threshold values of extent radius larger than 25″ and extent likelihood larger than 7, as supplied by the ML algorithm of SASS1. This set of cuts has been used successfully before (for details see, e.g., Fig. 7 in Ebeling et al. 1993). However, this method is not reliable in recovering all extended sources, since we find directly that several very extended sources are not recognized.

In order to better understand the completeness of the global identification process within the selection limits of the RASS1 Bright Sample, we have tried to exploit the complementarity of these two methods. (Note that most of the clusters in the sample have been found by both methods).

Let us assume that the two means of identification are uncorrelated, which is the case if clusters are missed by simple independent errors in the two techniques. This allows us to statistically infer the incompleteness of the sample in the following way. We define the set of clusters found by optical means as O, and the set found by X-ray extent as X.

The statistical independence of the two search methods allows us to write the combined probability of events O and X as

$$P(O \cap X) = P(O)P(X) \, . \tag{4}$$

Defining T as the parent sample [i.e., $P(T) \equiv 1$], we can relate the probabilities P to occurrences N in the following way: $P(X) = N(X)/N(T)$, $P(O) = N(O)/N(T)$ and $P(O \cap X) = N(O \cap X)/N(T)$. Substituting in equation (4), we obtain

$$N(T) = \frac{N(O)\, N(X)}{N(O \cap X)} \, , \tag{5}$$

and using the actual numbers in the subsets, $N(O) = 118$ $N(X) = 95$, and $N(O \cap X) = 83$, we find $N(T) = 135$. Consequently, the missing fraction of objects for our 130 clusters sample is $\sim 3.7\%$.

The assumption that the two methods of detection are uncorrelated is probably not strictly valid, since poorer and more distant clusters will be harder to find for both techniques. Therefore, the number calculated for the clusters missed is a lower limit to the missing fraction, but it is already reassuring that this fraction is as low as 3.7%.

6.3. *The* $\langle V/V_{\rm max} \rangle$ *Test*

As a final check, we have tested the spatial distribution of the bright clusters with the $V/V_{\rm max}$ method. Since our sample has different flux limits (§ 5.2), we have used the generalization of the $V/V_{\rm max}$ method (Schmidt 1968) given in Avni & Bahcall (1980). We have also assumed an Einstein–de Sitter cosmological model with $\Lambda = 0, q_0 = 0.5$, and $H_0 = 50$ km s^{-1} Mpc^{-1}. The derived $\langle V/V_{\rm max} \rangle$ is 0.49 ± 0.16, consistent with uniformity.

TABLE 3

MISSED ACO CLUSTERS

Name (1)	R.A. (J2000) (deg) (2)	Decl. (J2000) (deg) (3)	cr_{SASS1} (0.1–2.4 keV) (4)	z (5)	Reference (6)
A0194.....	21.3867	−1.5069	0.045	0.0178	1
A0514.....	71.9158	−20.4290	0.026	0.0730	1
A3164.....	56.4567	−57.0456	...	0.0611	2
A3223.....	62.1429	−30.8189	0.036	0.0601	3
A3716.....	312.8858	−52.7122	0.051	0.0456	2
A3733.....	315.4387	−28.0283	0.034	0.0386	2

REFERENCES.—(1) Struble & Rood 1987; (2) Abell et al. 1989; (3) den Hartog & Katgert 1996.

7. SUMMARY AND CONCLUSIONS

The aim of the present work was to derive an X-ray flux-limited sample of bright clusters of galaxies characterized by a high degree of completeness. It is based on a first cluster candidate sample derived in the ESOKP collaboration, belonging to the southern Galactic cap region ($\delta < 2.^{\circ}5$ and $b < -20^{\circ}$). We call this the RASS1 Candidate Sample, and it contains 679 sources.

We first performed a detailed reanalysis of fluxes for all sources in this RASS1 Candidate Sample by using the RASS merged data and the SRT method developed and discussed in Paper I.

We have applied to the RASS1 Candidate Sample various restrictive selections aimed at heavily reducing the sources of incompleteness. Our first selection set a lower limit of 150 s to the exposure time in order to avoid regions of sky where objects could have been missed because of the low sensitivity of the survey. In the second selection, we excluded crowded regions of the sky, i.e., the Galactic plane and the Magellanic Clouds, to avoid confusion problems affecting optical and X-ray catalogs. The third selection set a lower limit to the SRT count rate of 0.25 counts s^{-1} in the hard band. In setting the SRT count-rate limit, we investigated the behavior of a control sample of optically identified objects, namely, the EMSS sample reobserved in the RASS. These selections yielded an X-ray completeness in the derived sample of $\sim$95%. Such a high degree of completeness was reached at the expenses of drastically reducing the number of candidates in our sample, from 679 to 164.

We used our new data from the ESOKP, together with data drawn from the literature, to identify the selected candidates. After removing a number of false identifications, we produced a sample that contains 130 clusters with X-ray fluxes larger than $\sim 3.5 \times 10^{-12}$ ergs cm^{-2} s^{-1} and $z \lesssim 0.3$, covering a sky area of 8235 deg^2.

We then investigated the various sources of incompleteness and biases that could be affecting the RASS1 Bright sample. The key factor allowing us to constrain the incompleteness has been the application of a cut at a relatively high X-ray count rate. This action limits the bias against very extended X-ray sources (i.e., nearby clusters and groups). From our estimates we have also seen that this bias is kept under control for redshifts $\lesssim 0.08$, and eliminated for redshifts $\gtrsim 0.08$.

A statistical estimate of the completeness level of the identification procedure, based on the relative success rates of the two main methods of cluster identification (optical versus X-ray–based), indicates an incompleteness of $\sim$4% due to this source. Adding this to the incompleteness estimated from the flux-selection procedure, we obtain a global completeness for the sample that is better than 90%.

The log N–log S distribution is well described by a power law with slope $\alpha = 1.34 \pm 0.15$ and normalization $A = 11.87 \pm 1.04$ sr^{-1} $(10^{-11}$ ergs cm^{-2} $s^{-1})^{\alpha}$. A comparison between our result and previous measurements shows good agreement.

The sample discussed here should represent a useful database for a number of statistical studies of the properties of clusters of galaxies in the local universe. Finally, we should mention that the results presented here will be extended by the future developments of the ongoing ESOKP collaboration.

The authors would like to thank the *ROSAT* team at MPE, and H. T. MacGillivray at ROE and D. J. Yentis at NRL for having provided the COSMOS digitized optical sky survey catalogs. We also thank K. Romer for having allowed us to publish eight redshifts from the SGP project and P. Henry and C. Mullis for having provided two new redshifts. S. D. G. would like to thank P. Rosati, R. Della Ceca, and G. Zamorani for useful comments and discussions. Special thanks also to C. Izzo at MPE for his help in the data analysis. This research has made use of data provided by the NED and SIMBAD databases and of digitized optical images from the POSS and UK Schmidt sky surveys, obtained through the SKYVIEW facility. We also used data from the HEASARC online service and the *ROSAT* public archive. We thank all those who contribute to maintaining these databases.

REFERENCES

Abell, G. O., Corwin, H. G., & Olowin, R. P. 1989, ApJS, 70, 1
Allen, S. W., Edge, A. C., Fabian, A. C., Böhringer, H., Crawford, C. S., Ebeling, H., Johnstone, R. M., Naylor, T., & Schwarz, R. A. 1992, MNRAS, 259, 67
Avni, Y., & Bahcall, J. N. 1980, ApJ, 235, 694
Bahcall, N. A. 1975, ApJ, 198, 249
Bahcall, N. A., & Cen, R. 1993, ApJ, 407, L49
Böhringer, H. 1994, in MPE Rept. 256, Studying the Universe with Clusters of Galaxies, ed. H. Böhringer & S. Schindler (Munich: MPE), 93
———. 1995, in Ann. NY Acad. Sci., 759, Proc. Texas Symp. on Relativistic Astrophysics and Cosmology, ed. H. Böhringer, J. Trümper, & G. E. Morfill, 67
Böhringer, H., et al. 1998, in Proc. XIII IAP Meeting, Wide-Fields Surveys, ed. S. Colombi & Y. Mellier (Paris: IAP), in press
Briel, U. G., & Henry, J. P. 1993, A&A, 278, 379
Briel, U. G., & Pfeffermann, E. 1986, Nucl. Instrum. Methods, A242, 376
Brinkmann, W., Siebert, J., & Boller, T. 1994, A&A, 281, 355
Burg, R., et al. 1992, A&A, 259, L9
Collins, C. A., Guzzo, L., Nichol, R. C., & Lumsden, S. L. 1995, MNRAS, 274, 1071
Collins, C. A., Nichol, R. C., Romer, A. K., & Burke, A. 1997, ApJ, 479, L117
Crawford, D. F., Jauncey, D. L., & Murdoch, H. S. 1970, ApJ, 162, 405
Crawford, C. S., Edge, A. C., Fabian, A. C., Allen, S. W., Böhringer, H., Ebeling, H., McMahon, R. G., & Voges, W. 1995, MNRAS, 274, 75
Cruddace, R. G., Hasinger, G. R., & Schmitt, J. H. 1988, in Astronomy from Large Databases, ed. F. Murtagh & A. Heck (München: ESO), 177
Dalton, G. B., Efstathiou, G., Maddox, S. J., & Sutherland, W. J. 1994, MNRAS, 269, 151
Dalton, G. B., Maddox, S. J., Sutherland, W. J., & Efstathiou, G. 1997, MNRAS, 289, 263
De Grandi, S. 1996a, Ph.D. thesis, Univ. of Milan
———. 1996b, in MPE Rept. 263, Proc. Röntgenstrahlung from the Universe, ed. H. U. Zimmerman, J. Trümper, & H. Yorke (Munich: MPE), 577
De Grandi, S., Molendi, S., Böhringer, H., Chincarini, G., & Voges, W. 1997, ApJ, 486, 738
De Grandi, S., et al. 1999, ApJ Lett., in press
den Hartog, R., & Katgert, P. 1996, MNRAS, 279, 349
de Vaucouleurs, G., de Vaucouleurs, A., Corwin, H. G., Jr., Buta, R. J., Paturel, G., & Fouque, P. 1991, Third Reference Catalog of Bright Galaxies, Ver. 3.9 (Berlin: Springer)
Dickey, J. M., & Lockman, F. J. 1990, ARA&A, 28, 215
Douglas, J. N., Bash, F. N., Bozyan, F. A., Torrence, G. W., & Wolfe, C. 1996, AJ, 111, 1945
Ebeling, H., Edge, A. C., Böhringer, H., Allen, S. W., Crawford, C. S., Fabian, A. C., Voges, W., & Huchra, J. P. 1998, MNRAS, 301, 881
Ebeling, H., Edge, A. C., Fabian, A. C., Allen, S. W., Crawford, C. S., & Böhringer, H. 1997, ApJ, 479, 101
Ebeling, H., & Maddox, S. J. 1995, MNRAS, 275, 1155
Ebeling, H., Voges, W., Böhringer, H., & Egde, A. C. 1993, A&A, 275, 360
Ebeling, H., Voges, W., Böhringer, H., Edge, A. C., Huchra, J. P., & Briel, U. G. 1996, MNRAS, 281, 799
Evrard, A. E. 1997, MNRAS, 292, 289
Frenk, C. S., White, S. D. M., Efstathiou, G., & Davis, M. 1990, ApJ, 351, 10
Galli, M., Cappi, A., Focardi, P., Gregorini, L., & Vettolani, G. 1993, A&AS, 101, 259

Garcia, A. M. 1993, A&A, 100, 47
Gawiser, E., & Silk, J. 1998, Science, 280, 1405
Gioia, I. M., Henry, J. P., Maccacaro, T., Morris, S. L., Stocke, J. T., & Wolter, A. 1990, ApJ, 356, 35
Gioia, I. M., & Luppino, G. A. 1994, ApJS, 94, 583
Guzzo, L., et al. 1995, in Wide Field Spectroscopy and Distant Universe, ed. S. J. Maddox & A. Aragon-Salamanca (Singapore: World Scientific), 205
Henry, J. P., Gioia, I. M., Maccacaro, T., Morris, S. L., Stocke, J. T., & Wolter, A. 1992, ApJ, 386, 408
Heydon-Dumbleton, N. H., Collins, C. A., & MacGillivray, H. T. 1989, MNRAS, 238, 379
Huchra, J., Latham, D. W., Da Costa, L. N., Pellegrini, P. S., & Willmer, C. N. A. 1993, AJ, 105, 1637
Jones, C., & Forman, W. 1984, ApJ, 276, 38
Jones, L. R., et al. 1998, ApJ, 495, 100
King, I. R. 1966, AJ, 71, 64
Kitayama, T., & Suto, Y. 1997, ApJ, 490, 557
Lauberts, A., & Valentijn, E. A. 1989, The Surface Photometry Catalogue of the ESO-Uppsala Galaxies (Garching bei München: European Southern Observatory)
Ledlow, M. J., & Owen, F. N. 1995, AJ, 109, 853
Maccacaro, T., Gioia, I. M., Wolter, A., Zamorani, G., & Stocke, J. T. 1988, ApJ, 326, 680
Maccacaro, T., Wolter, A., McLean, B., Gioia, I. M., Stocke, J. T., Della Ceca, R., Burg, R., & Faccini, R. 1994, Astrophys. Lett. Comm., 29, 267
Mazure, A., et al. 1996, A&A, 310, 31
Murdoch, H. S., Crawford, D. F., & Jauncey, D. L. 1973, ApJ, 183, 1
Muriel, H., Nicotra, M. A., & Lambas, D. 1990, AJ, 100, 339
———. 1995, AJ, 110, 1032
NED Team. 1992, Redshift Obtained from Literature by the NED Team prior to November 1992, Report Vol. 11 (Washington: NASA), 1
Piccinotti, G., Mushotzky, R. F., Boldt, E. A., Holt, S. S., Marshall, F. E., Serlemitsos, P. J., & Shafer, R. A. 1982, ApJ, 253, 485
Postman, M., Huchra, J. P., & Geller, M. J. 1992, ApJ, 384, 404
Postman, M., & Lauer, T. 1995, ApJ, 440, 28
Quintana, H., & Ramirez, A. 1995, ApJS, 96, 343
Romer, A. K., Collins, C. A., Böhringer, H., Cruddace, R. G., Ebeling, H., MacGillivray, H. T., & Voges, W. 1994, Nature, 372, 75
Rosati, P., Della Ceca, R., Burg, R., Norman, C., & Giacconi, R. 1995, ApJ, 445, 11
Rosati, P., Della Ceca, R., Norman, C., & Giacconi, R. 1997, ApJ, 492, L21
Sarazin, C. L. 1988, X-Ray Emission from Clusters of Galaxies (Cambridge: Cambridge Univ. Press)
Schmidt, M. 1968, ApJ, 151, 393
Snowden, S. L., & Petre, R. 1994, ApJ, 436, L123
Stocke, J. T., Morris, S. L., Gioia, I. M., Maccacaro, T., Schild, R., Wolter, A., Fleming, T. A., & Henry, J. P. 1991, ApJS, 76, 813
Struble, M. F., & Rood, H. J. 1987, ApJS, 63, 543
———. 1991, ApJ, 374, 395
Teague, P. F., Carter, D., & Gray, P. M. 1990, ApJS, 72, 715
Trümper, J. 1993, Science, 260, 1769
Tucker, W. H., Tananbaum, H., & Remillard, R. A. 1995, AJ, 444, 532
Voges, W. 1992, in Proc. Satellite Symp. 3, ed. T. D. Guyenne & J. J. Hunt (ESA-ISY-3) (Noordwijk: ESA), 9
White, S. D. M., Efstathiou, G., & Frenk, C. S. 1993, MNRAS, 262, 1023
Yentis, D. J., et al. 1992, in Proc. Digitized Optical Sky Surveys, ed. H. MacGillivray & E. B. Thompson (Dordrecht: Kluwer), 67
Zabludoff, A. I., Geller, M. J., Huchra, J. P., & Vogeley, M. S. 1993, AJ, 106, 1273